72-9020

BLAIS, Roger Nathaniel, 1944-
THE ELECTRICAL BREAKDOWN OF HELIUM.

The University of Oklahoma, Ph.D., 1971
Physics, plasma

University Microfilms, A XEROX Company, Ann Arbor, Michigan

© 1971

Roger Nathaniel Blais

ALL RIGHTS RESERVED

THIS DISSERTATION HAS BEEN MICROFLIMED EXACTLY AS RECEIVED

Downloaded from SHAREOK. Persistent Handle URL: https://hdl.handle.net/11244/3170

THE UNIVERSITY OF OKLAHOMA

GRADUATE COLLEGE

THE ELECTRICAL BREAKDOWN OF HELIUM

A DISSERTATION

SUBMITTED TO THE GRADUATE FACULTY

in partial fulfillment of the requirements for the

degree of

DOCTOR OF PHILOSOPHY

BY

ROGER NATHANIEL BLAIS

Norman, Oklahoma

1971

THE ELECTRICAL BREAKDOWN OF HELIUM

APPROVED BY

Richard D. Fowler

Stanley E. Bugg F.

Stephen C. Whitmore

G. A. Day

S. B. Eliason

DISSERTATION COMMITTEE

PLEASE NOTE:

Some Pages have indistinct print. Filmed as received.

UNIVERSITY MICROFILMS

ACKNOWLEDGEMENTS

It is doubtful if anyone could write a dissertation without the help of many people. The fear of leaving out the name of someone who made a significant contribution does not absolve one from mentioning specifically those whose help and encouragement made it possible to complete this project. Dr. Richard G. Fowler conceived the experiment, found funds for its sustenance, gave counsel on its complexities and pushed me on to its completion.

An experiment, like an Aristotelian plot, has a beginning, a middle and an end. Those three stages were served respectively by Drs. Richard A. Day, Ian D. Latimer, and Masud Naraghi. Dr. Stanley E. Babb, Jr., contributed a great deal of his time to the solution of the electrostatic field problem. Dr. Day and Dr. Robert M. St. John have given assistance both in and out of the laboratory.

It has been said that most of a student's education comes from his fellow students. Dr. Gary E. Copeland, Dr. A. W. Johnson, Dr. A. R. Schaefer, Mr. R. T. Thompson, Mr. J. I. Mills and Mr. P. S. Liou have born witness to that statment. A special note of thanks must go to Robert P. Scott who has contributed greatly to the project with his electronic skill. The last Geoffrey Russell will always be remembered as an example of the type of knowledge and enthusiasm that a good physicist should possess.

In an experiment of this size many craftsmen, technicians and skilled workers were essential to its completion. Involved machine work was expertly done by Mr. Gene Scott, Mr. Cleve Christian, Mr. Woody Porter and the late James Hood. The entire project would not have been feasible without the herculean glassblowing efforts of Mr. Ron Stermer. The typing was well accomplished by Mrs. Mary Lou Stokes. I also wish to thank my father, Mr. E. J. Blais, for doing the final drawings that appear in the text.

Finally, one must recognize the need for cooperation in his personal life if an extensive graduate program is to be undertaken. It is time to publicly thank for more things that I could begin to mention, my parents, who have never failed to encourage me, and my fiancee, Mary Louise Leclerc, who has given me a reason to complete this work.

This project was financially supported by the United States Air Force.

TABLE OF CONTENTS

Page

ACKNOWLEDGEMENTS iii

LIST OF ILLUSTRATIONS. vi

Chapter

I. HISTORICAL INTRODUCTION. 1

II. APPARATUS AND PROCEDURE. 7

Wave Launching Apparatus 7

The Breakdown Tube. 8
The Power Supply. 16
The Vacuum System 19

Wave Speed Diagnostics 22

Wave Speed System Components. 24
Temperature and Density Diagnostics 36

III. WAVE SPEED ANALYSIS. 38

Computing the Electric Field 41
Comparison to Theory 46

Wave Temperature and Density Results. 49

IV. CONCLUSIONS AND SPECULATIONS 54

BIBLIOGRAPHY 57

APPENDIX A Shelton Theory. 59

APPENDIX B Wave Speed Raw Data 67

APPENDIX C Raw Electron Temperature Data 71

LIST OF ILLUSTRATIONS

Figure		Page
1.	Driver End of Breakdown Tube	12
2.	Cutaway View of Driver End of Tube	13
3.	The Breakdown Tube Circuit	17
4.	The Vacuum System	20
5.	Block Diagram of Wave Speed Device	23
6.	The RCA 7746 Photomultiplier	25
7.	Delay Gate Pulse	32
8.	z versus t and v versus z	39
9.	v versus z, proforce	42
10.	v versus E/p, antiforce	43
11.	Proforce versus antiforce	52

ABSTRACT

A revision of the electrostatic breakdown apparatus used by Haberstich was employed to generate waves for studies of wave speed, electron temperature behind the wave front and electron density for the purpose of investigating the Shelton one dimensional fluid-dynamical theory for field driven proforce or negatively pulsed electrode breakdown. Such measurements have been carried out in helium at applied electrode voltages from 6 kV to 42 kV of both polarities and over a pressure range of 0.3 Torr to 30.0 Torr. Wave speeds were measured using nuclear data handling techniques in which times of flight are measured by a time-to-pulse height converter calibrated against delay lines known to one nanosecond and the results are statistically compared by a multichannel analyzer. Temperatures were determined from a spectral line intensity technique and an absolute calibration yielded the electron densities. The results include the establishment of an exponential decrement rule for wave speed as a function of distance down the tube and a corresponding constant velocity changeover criterion, a confirmation of the functional form relationship between wave speed and applied electric field as proposed by Shelton but with a more complicated pressure dependence than that proposed by his one dimensional theory, and the presentation of extensive data which may be used for the future evaluation of theoretical refinements in the Shelton proforce theory and for the extension of the theory to the antiforce or positive electrode wave.

CHAPTER I

HISTORICAL INTRODUCTION

It has long been known that a gas of neutral particles can break down from a normally insulating state and become an ionized electrical conductor. Since man first observed this in the form of lightning he has learned to employ gaseous conduction in such useful devices as the fluorescent light and the welding arc. Though the process of gaseous conduction is well understood on both a macroscopic and a microscopic scale, the process by which a gas changes from insulator to conductor has only been partially investigated. The present work deals with an experimental study of the breakdown process when it results from the application of a large potential gradient to a gas.

By the beginning of the twentieth century the work of four men in particular had established that breakdown occurs by the progagation of a luminous wave through a gas with no mass motion. The first man to seriously study luminous pulses from low pressure chambers was Francis Hauksbee[1], who noted in 1705 that flashes of light emanate from the evacuated tube over the mercury column of a barometer when the instrument is vibrated. He attributed these mercury vapor pulses to effluvium falling out of the vacuum onto the walls of the glass tube. By 1835 Wheatstone[2] had speculated that when such breakdown occurs between

two electrodes it is actually traveling from one electrode to the other with a finite speed. Though his experiments with a rotating mirror neither confirmed nor denied this hypothesis, he did succeed in establishing that if such a wave exists, it must have a speed greater than 10^7 cm/sec. In 1874 W. von Zahn[3] looked for a Doppler shift in the spectrum of the luminous front. When he published his results five years later, he declared that any such shift was too small for his apparatus to detect. Von Zahn had established that such waves involve no mass motion. In 1893 J. J. Thomson[4] measured waves moving at one half the speed of light in a fifteen-meter long discharge tube. It appears now that Thomson actually observed a fast, bright return wave through the already ionized gas rather than the dimmer breakdown itself. Yet for the first time the finite velocity of what we might now call electron fluid-dynamical waves had been determined.

Though the first three decades of the twentieth century added little to the knowledge of these waves, a fundamental advance occurred when Beams[5] experiments lead him to propose a qualitative theory in 1930. All attempts to identify such waves with solutions to Maxwell's equations having proved fruitless, Beams proposed an idea consistent with the lack of mass motion. He theorized that electrons are the primary determinant of wave propagation. In short, he held that the asymmetry of the discharge tube causes the point of highest field intensity to be located at the pulsed electrode. Free electrons are then accelerated by the electric field until they attain energies sufficient for collisional ionization of the gas near the electrode. As a conductor the ionized gas can sustain no internal electric field. The potential of the electrode

then determines the potential of the entire ionized region. The strongest field is then located at the interface of the neutral and ionized gas, and the process continues the propagation of the interface into the neutral molecule region. This theory is still considered essentially sound. With this model in mind Snoddy, Beams and Dietrich and their later collaborators[6,7,8] began publishing in 1936 a series of experimental papers containing studies of wave speeds as a function of various parameters. Wave speeds increase, for example, with an increase in tube diameter and applied potential. As a function of pressure the speeds exhibit a maximum around a few Torr. By pulsing their tube up to 125 kV they were able to measure waves of one third the speed of light.

During this period of qualitative theory Schonland and Loeb studied gaseous breakdown in geometries other than long discharge tubes. Schonland[9,10] studied the speed of pilot streamers in the lightning discharge. Struggling with the inability to control experimental conditions in the discharge, he evolved no theory for streamer propagation in spite of developing a criterion based on energy conservation for their minimum speed. Loeb[11] and his colleagues studied corona discharges in a plane-anode, point-cathode geometry. Loeb's hypothesis is that photons emitted from the luminous wave front excite atoms in the neutral undisturbed gas. These excited atoms subsequently emit photons and the wave propagates by photoionization. This theory fails to explain propagation in an atomic gas and, in addition, has not yet had a satisfactory mathematical analysis. Similar analysis by Nelson[12] suffers from the same objections.

In recent years the study of breakdown has been marked by greater success in coordinating the results of experiment with quantitative theories of increasing sophistication. Fowler and Hood[13] reported in 1962 the observation in an electric shock tube of precursor waves that bear strong similarities to breakdown waves. In a companion paper Fowler and Paxton[14] offered a preliminary quantitative theory based on a three fluid model of electrons, positive ions and heavy neutrals. They used the fluid-dynamical equations for conservation of mass, momentum and energy of the three components, together with Poisson's equation and then sought solutions in which the luminous front is viewed as a shock wave in the electron fluid. This theory achieved reasonable agreement with experimental results even though it neglected energy loss due to inelastic collisions.

In 1964 Haberstich[15] did an experimental and theoretical study of breakdown waves of both polarities at applied voltages up to 10 kV in helium and argon at pressures from 0.1 Torr to 10.0 Torr. Though the theory he offered for explaining the structure and propagation of the wave is inadequate, the experimental work he did remains both innovative and phenomenologically sound. First, he contributed an appropriate geometry for the electrostatic field configuration with well defined grounds by enclosing his long straight tube with a coaxial metal cylinder. Second, he measured wave speeds as a function of both pressure and applied voltage by using photomultipliers and electrostatic probes. Third, he established the spatial coincidence of the probe detected disturbance and the photomultiplier detected luminous pulse. Fourth, he used the probes to determine the decrement of the potential at the wave

front as a function of distance down the tube. Finally, he determined the number density of electrons behind the front by using microwave interferometry.

In spite of all these advances made by Haberstich, several objections which can be raised to his results severely limit the possibility of comparing them to a quantitative theory. He never measured one parameter of paramount importance, the electron temperature. Of lesser significance is the questionable nature of his wave speed calibration since he used only the time base of a dual beam oscilloscope as a time standard and determined velocities by observing a single event. Finally, his gas purities are extremely dubious for he employed merely a mechanical fore pump to evacuate his system.

The most satisfying theory to date was proposed by George Shelton[16] in 1967. Following Paxton and Fowler's lead, Shelton used a three fluid model to analyze the case of a one dimensional wave traveling in the direction an electron would be accelerated by the applied electric field. Solving the problem in a coordinate frame moving with the wave front, Shelton used the principle of frame invariance to find analytic forms for both the elastic and inelastic collision terms in the energy and momentum equations. At Fowler's suggestion he introduced clarifying terminology designating those waves for which the external field accelerates electrons in the direction of wave propagation as <u>proforce waves</u>, and the case in which electron acceleration and wave propagation oppose as <u>antiforce waves</u>. Thus, Shelton's theory applies only to the proforce case, the case Haberstich called a negative ionizing potential wave. By applying appropriate boundary conditions Shelton solved the fluid-

dynamical equations simultaneously with Maxwell's equations. This ultimately leads to relations between wave speed, field strength at the front, electron temperature in the ionized region and number density of electrons behind the front. He predicted a minimum cutoff velocity for proforce wave propagation with a corresponding minimum field necessary to initiate breakdown. He neglected, however, to include the heat conduction, a quantity which perhaps determines the direction of wave propagation and may solve the riddle of why waves always travel from the pulsed electrode to the grounded electrode regardless of the pulse polarity. The failure to include heat conduction may have important ramifications in attempting to compare theory with experiment. A more detailed description of Shelton's theory can be found in The Appendix.

We now have a quantitative theory consistent with the qualitative theory proposed by Beams. It is the purpose of the present work to experimentally investigated the validity of the Shelton proforce theory and to provide experimental data for future analysis of the antiforce case.

CHAPTER II

APPARATUS AND PROCEDURE

In order to perform any scientific experiment it is first necessary to produce the phenomenon of interest under controlled conditions that can be reproduced at will, and second, necessary to measure the properties of interest related to that phenomenon. Therefore, a description of the apparatus constructed to meet these two needs is required.

Wave Launching Apparatus

The wave launching apparatus consisted of three main parts; the breakdown tube proper, the power supply and the vacuum system. Each of these was equipped with control mechanisms to guarantee the repeatability of each measurement performed. The breakdown tube consisted of a long straight Pyrex tube filled with a gas to be tested, a launching electrode to initiate the wave, a bleeder electrode to remove electrons from the walls, an electrostatic ground array to provide a simple known geometry for the electric field and to shield the wave from stray fields, a series of light pipes to locate permanent viewports on the tube, a rail and cart system to firmly support the optical diagnostics and a scantling table to support the whole affair. The power supply contained a voltage doubler circuit to rectify and step up the line voltage, a capacitor to store charge for the firing, a spark gap to apply a clean step function

of voltage to the tube electrode and the necessary controls to adjust the spark gap voltage, regulate the rate of firing and to discharge the capacitor to ground at the end of a data run. The vacuum system consisted of the pumps necessary to clean old gas from the tube and set the desired pressure of the gas introduced, cold traps to maintain the purity of the gas during a run, a gas bottle and regulator for introducing the high purity gas and gauges for measuring the system pressure and searching for leaks.

The Breakdown Tube

The Pyrex tube. The breakdown tube was a twenty-four foot long straight piece of Pyrex 7740 pipe line tubing with a five centimeter inner diameter and a five-eighth centimeter wall thickness. It was fabricated by sealing three sections of eight foot long pipe together so that no O-ring or metal clamps would upset the flow of the wave or distort the symmetry of the field experienced by the wave. The eight foot sections were made by cutting one foot from each end of a standard ten foot section in order to remove the double tough region at both ends. Although this was a necessity of fabrication it had the added advantage of assuring the homogeneity of the glass composition and its dielectric properties. At each end of the tube a reducing seal was made to constrict the diameter of the tube from 50 mm to 25 mm. This smaller diameter tube was used so that the insertion of electrodes and the connection to the vacuum system could be done in place rather than on the glassblower's lathe. The tube was supported at three foot intervals by specially shaped blocks of Styrofoam. Styrofoam was chosen because,

being mostly air, its dielectric properties are close to those of air. It contributed, thus, little to the distortion of the electric field. These supports firmly held the tube along the axis of a circular cylindrical electrostatic ground array.

The electrostatic ground. The electrostatic ground was designed to minimize corona losses as well as provide field symmetry. Twenty 1¼ inch diameter aluminum pipes were evenly arranged parallel to one another to form the walls of a right cylinder with the center of each pipe six inches from their common cylindrical axis. The pipes each were drilled and screwed to six polished cast-aluminum rings that each had twenty notches milled on their inner surface to accomodate the pipes. The holes in the pipes were filled with aluminum and the seams were hand polished so that no sharp edges were available for corona. At each end of the twenty pipes a hemispherical plug was also inserted for the same purpose. The rings had been cut along a major diameter so that after assembly the entire cylinder could be split lengthwise like the top being removed from a twenty-four foot long coffin if one needed to gain access to the Pyrex tube. When the two halves of the cylinder were together the halves of the rings connected with each other by a pin and socket arrangement. It was possible to mount a hemispherical cap of spun sheet aluminum at either end of the ground array. The sharp edge of the sheet was embedded in an additional cast aluminum ring which served as a mount to hold the ring in place. Through the liberal use of silver conducting paint and undergraduate labor for polishing it can be stated that every portion of the surface was smooth and curvilinear.

Operation mechanism. The entire assembly was mounted on a scantling table made of kiln dried birch and coated with marine spar varnish. With an eye toward possible future use of the device in which fields external to the ground array might not be small, the investigators decided to glue and peg the table together without the use of nails. A wooden saddle on top of the table held the bottom half of the longitudinally split ground array. The Pyrex tube rested at the array's axis on its Styrofoam mounts which in turn rested on the inside of the bottom half of the ground array. When the cylinder was complete and in position for operation, the top half of the ground array rested on the bottom half. When the array was opened to gain access to the tube, the top ten pipes and their supporting half rings could be suspended by ropes and pulleys from a mount permanently installed in the laboratory ceiling.

Diagnostic access. Beyond mechanical strength and stability, a design using parallel pipes has an inherent advantage over a singly split large cylinder in that it affords multiple diagnostic access at a given longitudinal position along the tube. Since diagnostics are movable in the z direction, it becomes important to be able to reproduce their positions exactly. Variations as large as ten per cent were found in measured times of flight when the phototubes were merely mounted uncollimated opposite the nearest slot without using fixed position viewports. Such viewports were therefore provided by masking the tube itself, observing through light pipes, and clamping the phototubes in position. The Pyrex tube was covered with black paper with half centimeter openings at quarter meter intervals along the horizontal axis of

the cylindrical tube. Alternate slots, those at distances from the electrode of 1.75 m, 2.25 m, 2.75 m, etc., were equipped with 0.75" diameter lucite light pipes permanently clamped into position with one end butting up against the discharge tube and the other end sticking out between the aluminum pipes. The lucite light pipes were used for wave speed studies only. The slots at 2.0 m, 2.5 m, 3.0 m, etc. were left free from light pipes so that electron temperature and density studies could be accomplished without the intervening lucite as an added and useless component of the optical system. The entire array of metal pipes was swaddled in black cloth with only small holes for the optical instruments to peer through. On the scantling table an aluminum rail ran parallel to the tube on which were mounted carts to support the optics. Interchangable mounts were made to solidly attach to the cart a photomultiplier or a monochromator. The carts could be locked down at fixed positions by finger screws and the position along the rail at which to lock them could be located by touch even in the dark. A touch code stamped on the rail much like Braille let one be certain of which viewport he was using in the darkness.

Electrical properties of the breakdown tube. An electrode designed to facilitate wave initiation was sealed into one end of the tube by a wolfram glass to metal seal. Figures 1 and 2 will illustrate the structure of this end, the driver end, of the discharge tube. Because wave initiation demands the presence of electrons in the vicinity of the electrode or point of highest field several designs exploiting field emission were tried. The most successful shape resembles a florist's

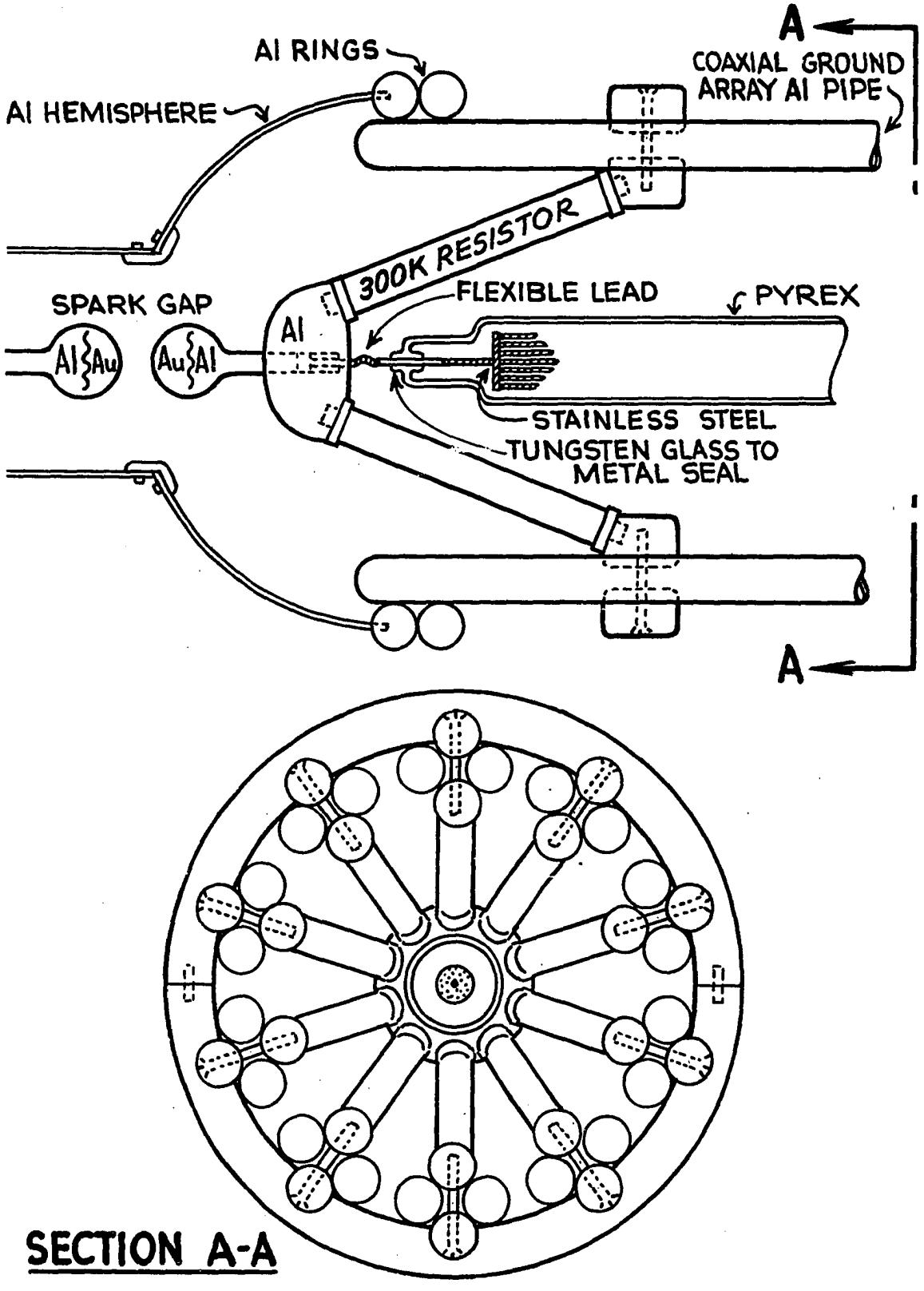

Figure 1. Driver end of breakdown tube.

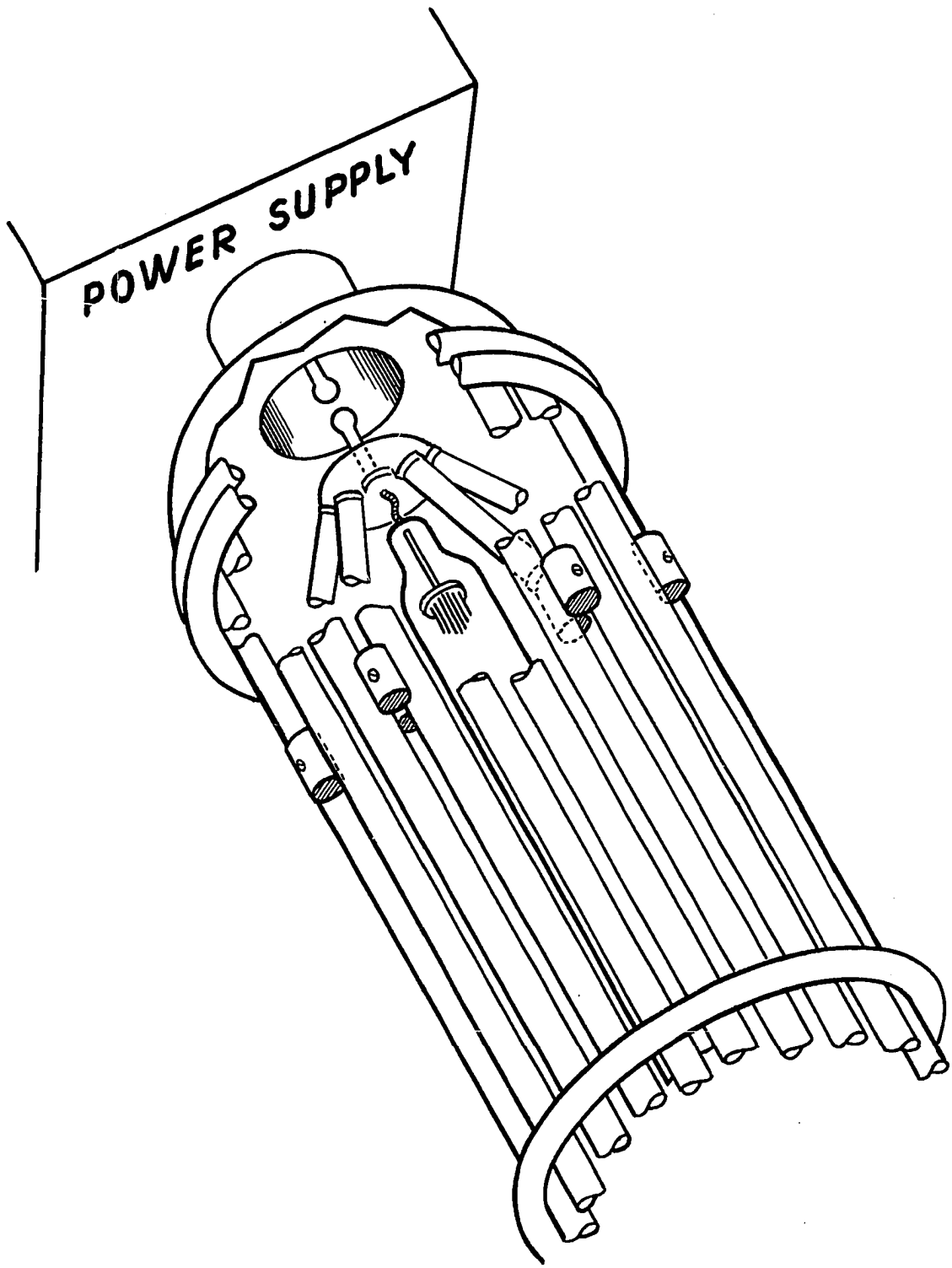

Figure 2. Cutaway view of driver end of tube.

frog with sharp pointed spines. The longest spines were in the middle so that their full effect on field emission would not be diminished by those farther from the central axis as would have been the case with a flat faced electrode.

A second electrode was mounted at the other end of the tube. It was essentially a straight piece of wire used to make certain that the electrons that had gone to the walls during the discharge were bled from the tube between firings. During the early stages of experimentation this electrode was connected to ground by a 24 kΩ resistor, but this caused an extremely bright glow discharge to light up the tube after the breakdown wave had traveled from end to end. This brilliance threatened to harm the multiplier phototubes, so during most of the data runs this electrode was not connected to ground. Its external end was merely covered with a block of solid aluminum, rounded to reduce corona. When this same end of the tube was fitted with its spun hemispherical cap as described above, it was found that arcing would occur between the external stub of this unused electrode and the cap, when the tube was pulsed to high voltages. Thus, for most of the experiments this cap was also removed. It should be mentioned that speed measurements performed with a Tektronix 555 dual beam oscilloscope indicated that these two alterations, disconnecting the electrode and removing the cap, did not alter the speed of the breakdown wave itself. It appears that until the wave nears the far end of the tube it is insensitive to the nature of the field in that vicinity.

Before going further it ought to be noticed that the field inside such an array of pipes is geometrically fluted unlike the field

inside two coaxial cylinders. Along the axis of the cylinder, however, this is hardly noticeable. If one considers the propagation of the wave down the tube to be similar to the charging of an unterminated coaxial transmission line, he can calculate the appropriate sizes and positions for twenty parallel conductors symmetrically arranged about a central inner conductor so that the electrical parameters of the transmission line are identical to a given coax. King[17] in his book on transmission line theory gives the following criterion. If the inner conductor has radius a, and there are 2N outer conductors each of radius a_1 and located at a distance b from the inner conductor, then the 2N conductors approximate an outer coaxial cylinder of radius b provided

$$a_1 = \frac{b}{2N} \quad .$$

For the case under discussion this criterion is satisfied to within a factor of two. This simply means that the ground array is a coax, but that the distance from any given pipe to the glass tube is not the same as the electrically corresponding coaxial cable's outer radius. An empirical measurement was made of the capacitance per unit length of ground array and the value determined was 33 picofarads/m.

At the driver end a spider array of ten 300 kΩ resistors as shown in Figs. 1 and 2 were symmetrically mounted forming a cone about the electrode. These low inductance carbon resistors served the double function of providing mechanical support for one side of the firing spark gap and of providing an electrical path to ground so that the spark gap would discharge with stability and reliability. In addition,

one of the resistors was made part of a 6000 to 1 resistive voltage divider that could then be used to monitor the electrode voltage. Once this had been calibrated against a Tektronix high voltage probe it was used to measure the electrode voltage and to provide a start pulse for whatever other electronics might need it.

The Power Supply

The power supply had to be capable of switching an electrically noise free step potential on the order of 50 kV onto the electrode with a pulse rise time of about 10 nanoseconds. While the description of how this was accomplished is brief, the building and rebuilding of the power supply was the single most time consuming aspect of the entire project. The difficulty resulted from attempts to use high speed vacuum relays for pulsing the tube. It turns out that as the relay contacts close the field between them becomes high enough for arcing to occur. Even the low pressure regime in which the relays operate fails to alter this arcing and the subsequent electrical noise generated by the spark. This difficulty was eventually overcome by applying a classic method, a discharge across a spark gap.

The operationally significant parts of the power supply can be seen in Fig. 3. A more detailed description follows. Sixty cycle A.C. entered the power supply through a Sola isolation transformer, a main switch, an ammeter and a variable transformer and was then applied to the primary of a Plastic Capacitor 50 kV Power Pak. The Power Pak is a sealed unit containing a step-up transformer, two silicon rectifiers and two high voltage capacitors all connected as a voltage doubler

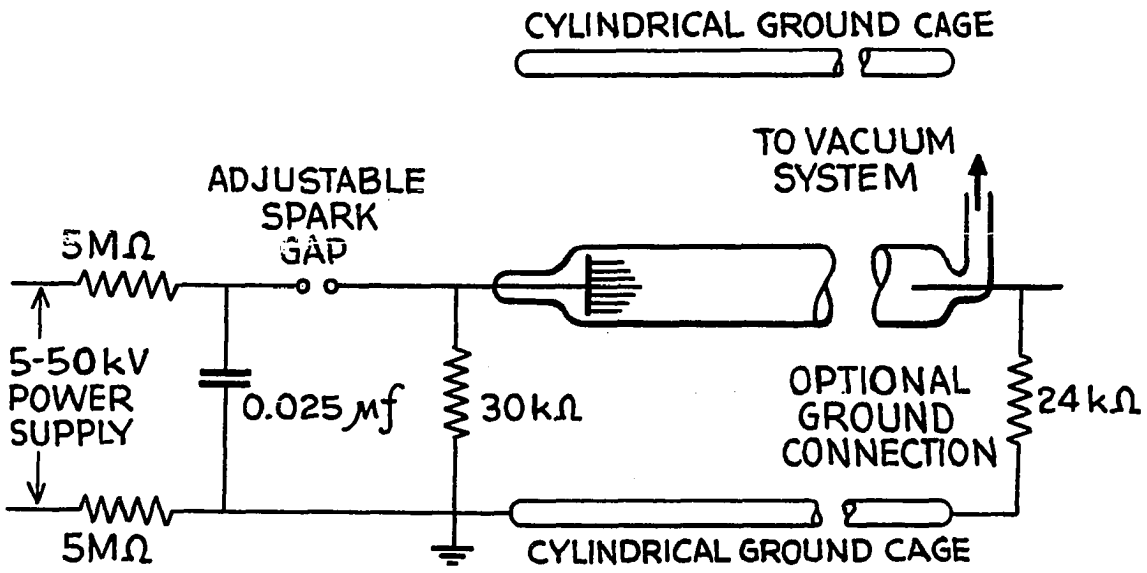

Figure 3. The breakdown tube circuit.

circuit. The output voltage is rectified with a very small ripple factor and is proportional to the input voltage. Controlling the input voltage from 0 to 110 V A.C. yields output voltages from 0 to 50 kV D.C. This output voltage was applied through a 10 MΩ charging resistor to a 0.025 microfarad capacitor capable of withstanding such voltages. The Power Pak was mounted on a lazy-Susan like rotating platform. This allowed for the interchange of the output high voltage stand-offs where they connected to the charging capacitor. One side of the capacitor connected to ground; the other side fed the spark gap. The entire affair was enclosed in a sheet metal box to help solve the difficult problem of shielding.

The spark gap itself was constructed from two aluminum spheres with inlaid gold on the active surface between them and a mechanical control system. The sphere on the tube electrode side was fixed in position, but the sphere on the power supply side could be moved by a crank so that the gap separation could be varied at will, thereby varying the voltage applied to the electrode. The spark gap control operated in concert with the variac that controlled the ultimate voltage available off the secondary of the Power Pak. Together these two controls allowed one to select not only the voltage applied to the tube, but also the pulse repetition frequency or PRF. Most data were acquired with a PRF of about one pulse per second.

One further portion of the circuit was the dumping mechanism. This allowed one to draw the charge off the main capacitor by shorting it through a heavy resistor. In this part of the circuit a use was

finally found for the high voltage relays with which we had unsuccessfully tried to fire the tube.

The Vacuum System

Description of the system. Purity of sample gas was the determining factor in vacuum system design. As is apparent in Fig. 4, the system was made entirely from glass without O-ring seals and used pumps with a very low ultimate pressure and Hy-Vac stopcocks with Apiezon Type N stopcock grease. Specifically, the individual components were a Duo-Seal model 1402 mechanical fore pump, an NRC type HSA two inch air cooled diffusion pump, a Matheson regulator, an NRC 531 thermocouple gauge head and an NRC Bayard-Alpert 563 ionization gauge head both of which were controlled by an NRC model 831 TC/ionization gauge station. A McLeod gauge was calibrated and installed to give absolute pressure readings. As a result the two electronic gauges were used mostly to simplify the pump out and filling procedures by direct constant monitoring. The McLeod gauge was the only standard employed for all pressures recorded as data. The ultimate system pressure was well below 0.1 micron and perhaps as much as an order of magnitude lower. The total volume of the system was thirteen liters, nine of which were the tube itself.

Gas handling procedure. The procedure for filling the tube with gas began with pumping the tube down to ultimate pressure as read on the most sensitive McLeod gauge scale. Then the system was allowed to pump for one additional hour. Then the stopcock between the system and the pumps was closed and the pressure was read at intervals to

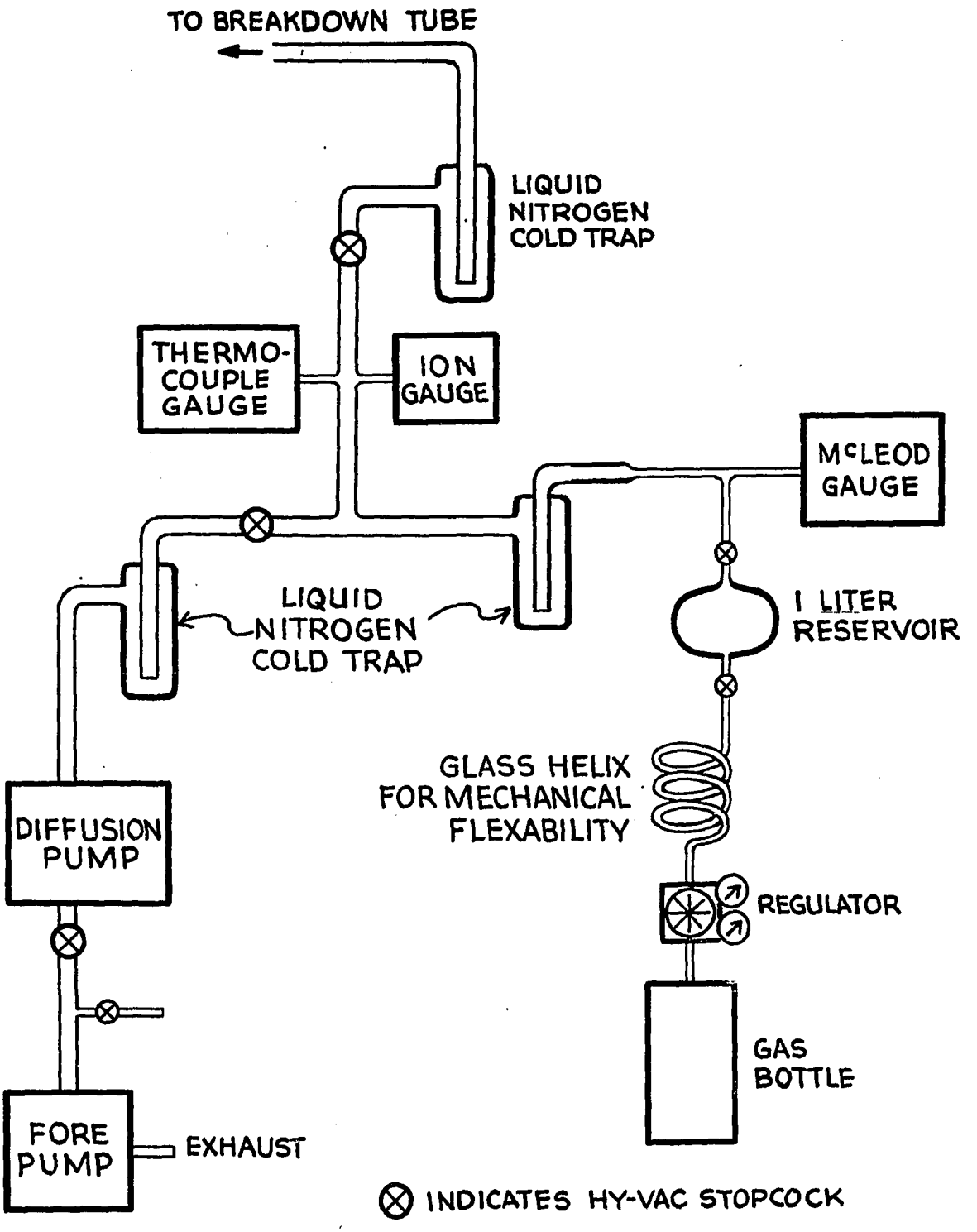

Figure 4. The vacuum system.

determine if any leaks were present. A short initial rise in pressure could be attributable to outgassing, but if it continued a leak was suspected. In an all glass system such as this leaks could normally be attributed to a stopcock in need of cleaning and regreasing. Matheson research grade helium, containing no more than 2 PPM impurities, mostly neon, was injected via the regulator which had been pumped out to the bottle valve. This gas filled a one liter reservoir to just over one atmosphere of pressure. The entire system was then flushed out with helium and the reservoir was refilled with fresh gas. The discharge tube and the pumps were then closed off and the portion of the system containing the McLeod gauge and its associated manometer was filled with new gas. By using the manometer and knowing that the volume of this portion of the vacuum system was one twenty-second part of the volume of the portion of the system containing the discharge tube plus this manometer section, it was easy to fill the tube approximately to any desired pressure. Next, the bottom end of the liquid nitrogen cold trap between the discharge tube and the tube stopcock was chilled. A few minutes later when impurities had frozen out on the bottom of the trap, the rest of the trap was immersed in liquid nitrogen. The two stage process ensures that as the nitrogen level drops by evaporation the worst impurities will remain in the trap. Then, after a few moments to equilibrate, the tube pressure was accurately measured by the McLeod gauge and the stopcock on the breakdown tube was closed. The slight pressure gradient resulting from the natural pumping action of a cold trap was simply ignored. The added step in the gas filling and cleaning procedure was to fire several hundred antiforce waves in

the tube before the final gas filling so that electron bombardment of the walls and especially the stainless steel electrode could clean them.

Wave Speed Diagnostics

Wave speeds were measured by a method which to this author's knowledge has not been previously applied to the study of such gaseous discharges, a method which offers high absolute time resolution, statistical compilation of the results of many events and the elimination of the need for carefully matched photomultipliers. Two photomultiplier tubes, henceforth frequently called PM's, were set before half centimeter slotted viewports distributed at quarter meter intervals down the tube. The PM signals were then applied by timed cables to the start and stop inputs of a time to pulse height converter, henceforth known as a TPHC. The output pulse was voltage analyzed by a multichannel analyzer, or MCA, which could assemble and store the results of a statistically significant number of events. Data on time delays between observation ports were read out on either an oscilloscope or a teletype. The entire apparatus could be calibrated against delay lines known to roughly one nanosecond. The experimental procedure was to leave the start or trigger PM at a fixed position along the tube and to move the stop PM to successive ports, obtaining a distance versus time, or z vs t, plot. On such a graph wave speeds appear as slopes. Added sophistication was gained by gating the TPHC start input against the applied voltage on the tube. Thus, start signals from slow waves which formed only after a significant decay in applied voltage were not counted. Fig. 5 is a block diagram of this sophisticated stopwatch.

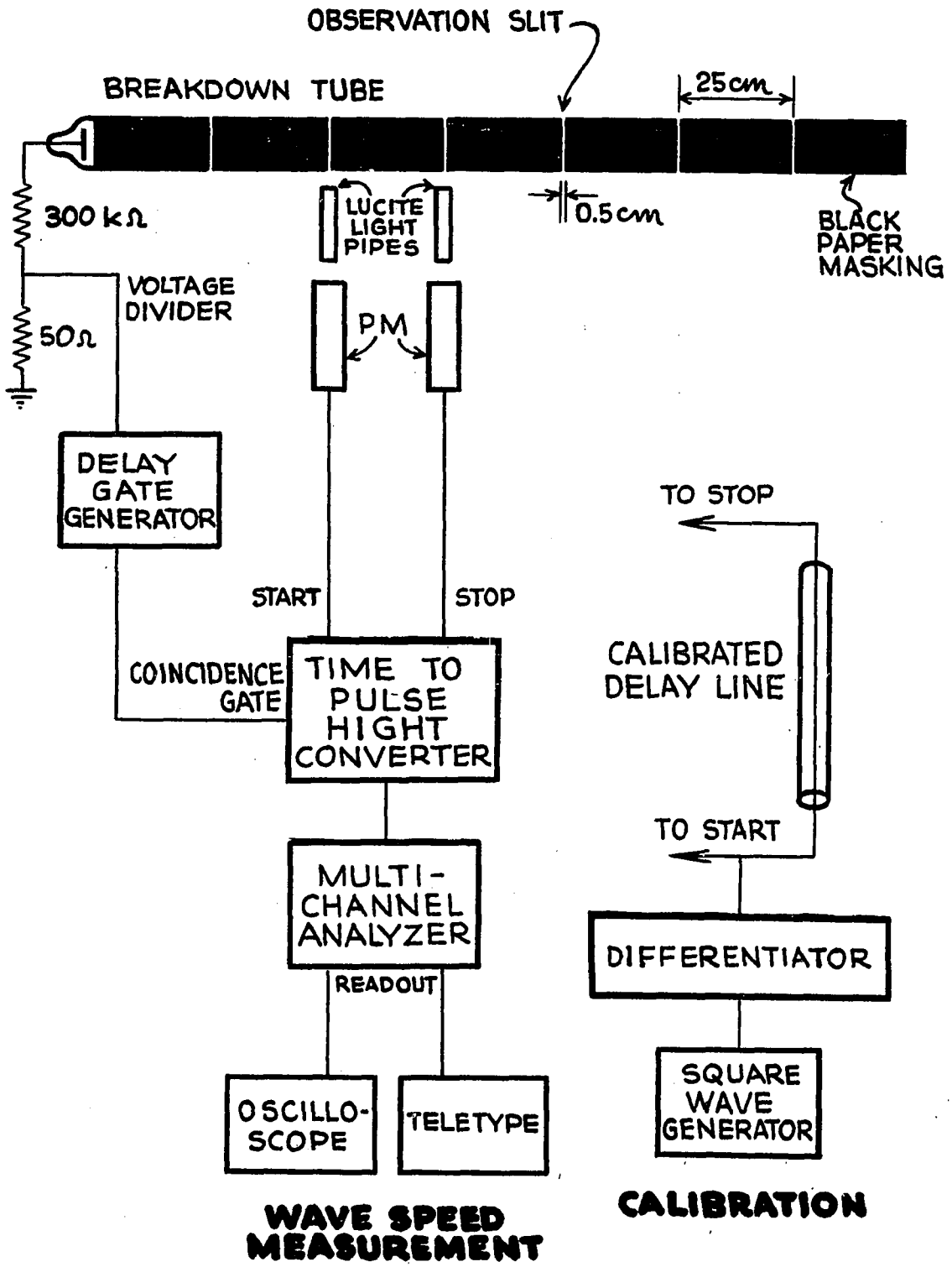

Figure 5. Block diagram of wave speed device.

Wave Speed System Components

Photomultipliers. Two different types of phototubes were used to supply the start and stop signals for measuring the time of flight of the waves. The procedure of keeping one, the start PM, at a fixed position and moving the other from viewport to viewport assures that differing rise times on the two phototubes do not upset the validity of the data. The first piece of information measured must, of course, be thrown out as an absolute time of flight value. But all subsequent times are measured by employing the same PM to give a stop pulse at the two different locations. On any given run an attenuation in light intensity as the wave progresses down the tube is compensated for by increasing the applied voltage on the PM. This was seldom necessary due to the use for wave speed studies of unfiltered light which had sufficient luminous intensity to allow the operation of the phototubes at voltages well below their maximum sensitivity. This fact coupled with the high rise time of the tubes made time of flight measurements on the system relatively insensitive to either the applied PM voltage or the absolute luminous intensity at any point along the tube. Several quick checks with interference filtered light convinced the writer that white light and monochromatic light both give the same measured wave speed.

The trigger or start PM was an RCA 7746 mounted at the lucite light pipe 1.75 m from the driving electrode in an aluminum housing with the circuit shown in Fig. 6. The 7746 is a ten stage head on, in line, spherical faceplate tube with a maximum spectral response at

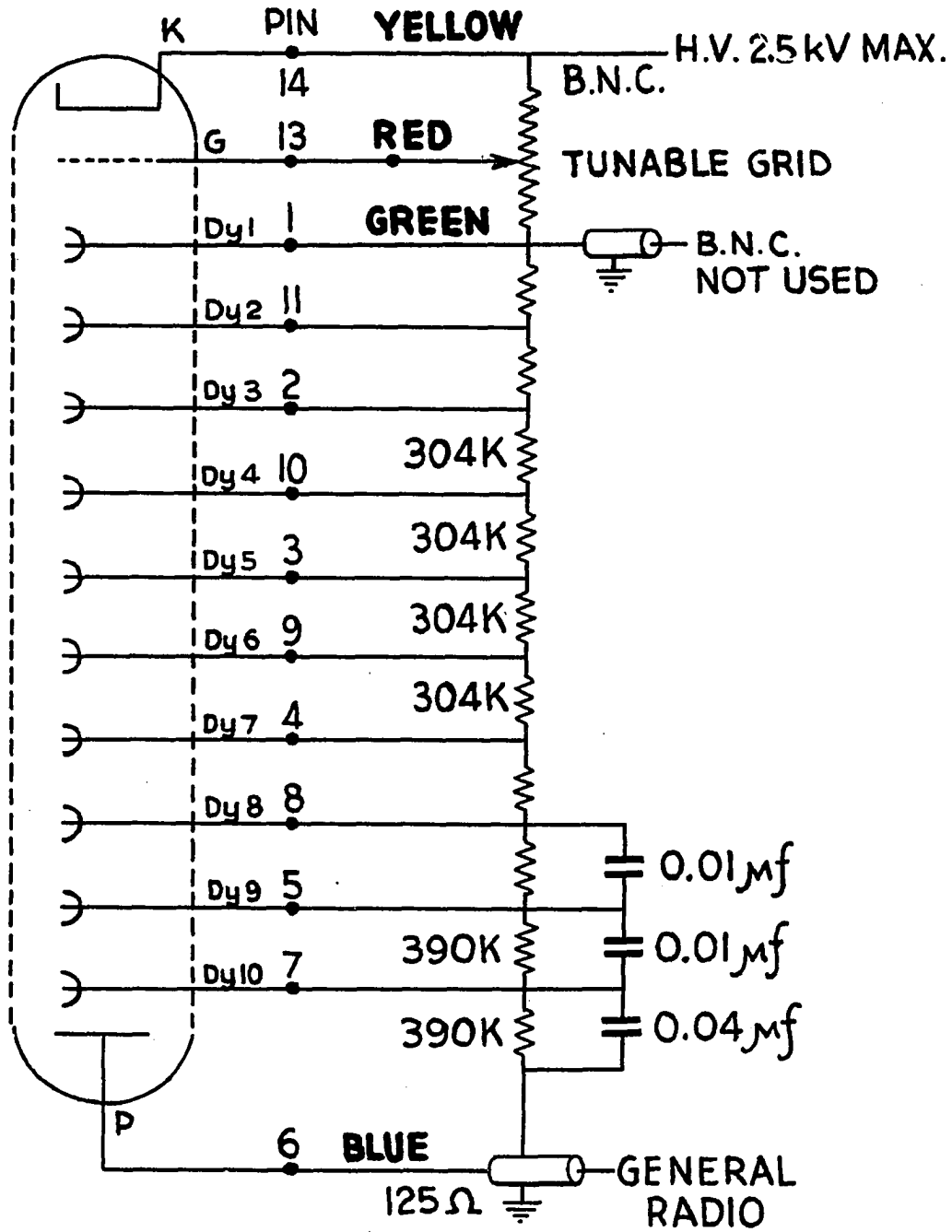

Figure 6. The RCA 7746 photomultiplier.

4400±500 Å. It has a semi-transparent spherical circular cesium antimony photocathode with S-11 spectral response, copper-beryllium dynodes and a Corning #0080 lime glass window. The maximum cathode to anode voltage rating is 2500 V; the anode pulse rise time is 2.3 ns (ns ≡ nanosecond) and a luminous sensitivity at the anode of 130 amps per lumen. Most data were collected with the cathode to anode voltage at about 800 V, well below the maximum allowed. The can in which the PM was mounted enclosed it completely except for a small hole 3/4 inch in diameter in the center of the faceplate. This hole exactly matched the size of the light pipe that butted up to it. The signal was sent on a coax cable with intrinsic delay time of 13.5 ns to the start input of the TPHC.

It should be noted at this point that great precautions were taken to be certain that no stray background room light entered the PM. For both phototubes a black rubber collar extended from the cylindrical walls of the PM container coaxially around the light pipe up to the black cloth covered wall of the electrostatic ground array. In addition all data was taken with the room lights completely off and the windows blacked out.

The second or stop PM was an RCA 8575 mounted in a standard ORTEC 264 photomultiplier base with a mu metal magnetic shield. The 8575 is a twelve stage head on, in line tube with a plano convex window of Corning #7740 Pyrex and a bialkali spectral response with a peak sensitivity at 3850±650 Å. Its photocathode is $(CsK)_3Sb$ with Be-O-Cs dynodes on a copper-beryllium substrate. This tube has a maximum cathode to anode voltage rating of 3000 V, and an anode pulse rise time

of 2.7 ns with a luminous sensitivity of 300 amps/lumen at the anode. The ORTEC 264 base circuit has both a linear output and a fast logic pulse together with a preamplifier circuit that was not used for our purposes. All data were acquired with the linear output. The tube was enclosed in an ORTEC magnetic shield and fitted with a brass cap and black rubber collar that afforded it identical protection to that given the other PM.

The second PM like the first was mounted on a cart and rail assembly, but unlike the first was moved from station to station. As mentioned above, it was a simple matter to move the second tube a half meter to the next station and align it with the light pipe by touch even in total darkness. The linear output of the PM was connected to the stop of the TPHC by a cable of intrinsic delay of 32.0 ns. The cable was longer than the one on the 7746 for two reasons. First, because it took 18.5 ns longer for the pulse to travel down its cable to the stop gate than for the corresponding cable delay of the start gate, it was not necessary to worry that a difference in rise time on the phototubes coupled with a fast wave and a short distance between the two observation ports could cause the stop pulse to arrive at its TPHC input before that start pulse could get to its input. Second, the greater length of the stop cable was necessitated by the physical need to move the stop PM to various positions.

The time-to-pulse height converter. When the PM signals arrived at the TPHC inputs they encountered a standard ORTEC model 437. It accepts negative pulses on its 50Ω impedance start and stop inputs if their amplitudes exceed 250 mV and if their duration exceeds 2 ns.

There are fifteen switch selectable time ranges with full scale times from 50 ns to 80 μs. Time resolution is to 0.01 per cent of the full scale range with 2 per cent differential linearity from 10 per cent of full scale to 100 per cent of full scale, and 0.1 per cent integral linearity. The output is a positive leading bipolar square pulse from 0 to V_{max} volts in amplitude in the open circuit. It is possible to set V_{max} to any desired value between 3 V and 10 V to yield a convenient calibration. The start signal can be gated in either a coincidence or anti-coincidence mode by a positive DC coupled pulse of amplitude greater than 2 V. During the experiment the gate was used in the coincidence mode. That is to say that unless the gate pulse was on no signal would be accepted at the start gate. The range seldom extended beyond two microseconds full scale. We shall return to the subject of the delay gate shortly, but first we must describe what happens to the pulse we now have, a pulse of voltage amplitude proportional to the time delay between its two input pulses.

The multichannel analyzer. A Nuclear Data series 1100 analyzer system measured, compared and stored the bipolar pulses from the TPHC. This analyzer or MCA consists of four modules that like the TPHC, delay gate generator and delay amplifier all plug into an ORTEC 401A-402A NIMBIN power supply. One of the four modules, the power supply for the other three requires no additional comment. The second module, the memory which stored the results of the measurements, is of interest only to the extent that it, like the entire analyzer system, was never taxed by either the speed with which data entered it or the absolute number of data bits it had to handle and store. Designed for fast

nuclear experiments, the pulse repetition frequency of about 1 pps and our total number of counts, always less than a thousand, never approached the limits of its capacity. The third module was an analog to digital converter, or ADC. It changed the incoming pulse to a series decimal digitalized version capable of being handled by the fourth and final module. The ADC assigns each incoming pulse a number from one to two hundred fifty-six. Each number corresponds to a voltage window or channel such that the number n (i.e. the nth channel) must be of a voltage V that satisfies the inequality

$$V_n \leq V < V_n + \Delta V$$

while and incoming pulse of voltage V' assigned the number n+1 will satisfy

$$V_{n+1} \equiv V_n + \Delta V \leq V' < V_{n+2} \equiv V_n + 2\Delta V \quad .$$

These numbers then are fed to the fourth component, the data handling module, which functions on a command to either store the pulse, read out the stored pulses or turn on and off the analyzer according to its own internal clock.

The data stored in the analyzer could be continuously monitored as it was accumulated by watching an analog output on a Tektronix RM 503 oscilloscope. The channel numbers from 1 to 256 are fed into the horizontal sweep of the scope so that each channel is displayed as a dot along a line. To facilitate interpretation every tenth channel appears as a brighter dot. The acquired data are fed into the vertical input so that an event recorded in the nth channel appears on the scope as the nth dot jumps to a distance Δy above the line. If m events have

been recorded in channel n, the dot for that channel is a distance $m\Delta y$ above the baseline. Thus, a graphic display of the data is constantly available so that by seeing the number of channels into which data falls and the distribution of points among the channels, the experimenter can determine immediately the relative statistical spread of the data. If the waves being measured were all of the same speed, all data would then fall into several contiguous channels with most of the counts in the middle one. If the waves showed great variability in speed, they might be spread out over a dozen channels, or in an extremely bad case, over fifty channels perhaps with a definite skew. This would always indicate that something was wrong with the equipment or that a much larger sample was needed.

The ability to directly monitor the output of the MCA allows the experimenter the option of altering the procedure when the data appear useless. If the data were badly spread and the possibility of gross system malfunction had been eliminated then the experimenter might choose to use the delay gate generator to improve the results as described below, and failing that, he can at least use the teletype to read out the data in digital form for later statistical analysis. If the data spread is small, however, a considerable saving of time can be achieved by reading the results directly off the oscilloscope. If all data fall into five channels, it is good enough to record on a pad which channel had the most counts and how the counts were spread. The ORTEC 222 teletype page printer and tape punch can waste valuable time printing out endless rows of zeroes.

The delay gate generator. The unique capabilities of the delay gate generator contributed in many cases to the significant improvement of the data. This ORTEC 416A module accepts either a positive or a negative pulse and then produces any one of three desired output pulses. The positive input had to be greater than two volts and of duration greater than 25 ns, while the negative input had to be greater than 250 mV and 2 ns. The output of importance to the present work was a positive square wave with a delay time between the input signal and the output onset of t_d in a range from 100 ns to 110 μs, and with a pulse duration of t_g in a range from 400 ns to 4 μs. The diagram below will clarify the following discussion. The values of t_d and t_g were continuously variable by potentiometer over the ranges specified. The amplitude of the gate pulse was variable from 2.5 V to 10.0 V which easily satisfied the requirements for the gate pulse needed by the TPHC.

The necessity of using the generator (DGG) can be seen by studying Fig. 7. Most of the statistical variation in wave speed was caused, it may be assumed, by the random variation in the time t_i between the application of voltage to the discharge electrode and the actual initiation of the breakdown wave. It is possible to make a reasonable agrument for attributing this randomness to fluctuations in the residual ionization. Regardless, it was experimentally noticed that the randomness deminished as the applied electrode voltage was increased or as the gas pressure was raised. At pressures below 1 Torr and potentials below 12 kV the randomness became sufficiently great to require very long data runs. It afflicted the anti-force data more severely than the proforce. At 0.3 Torr it had wiped out all useful

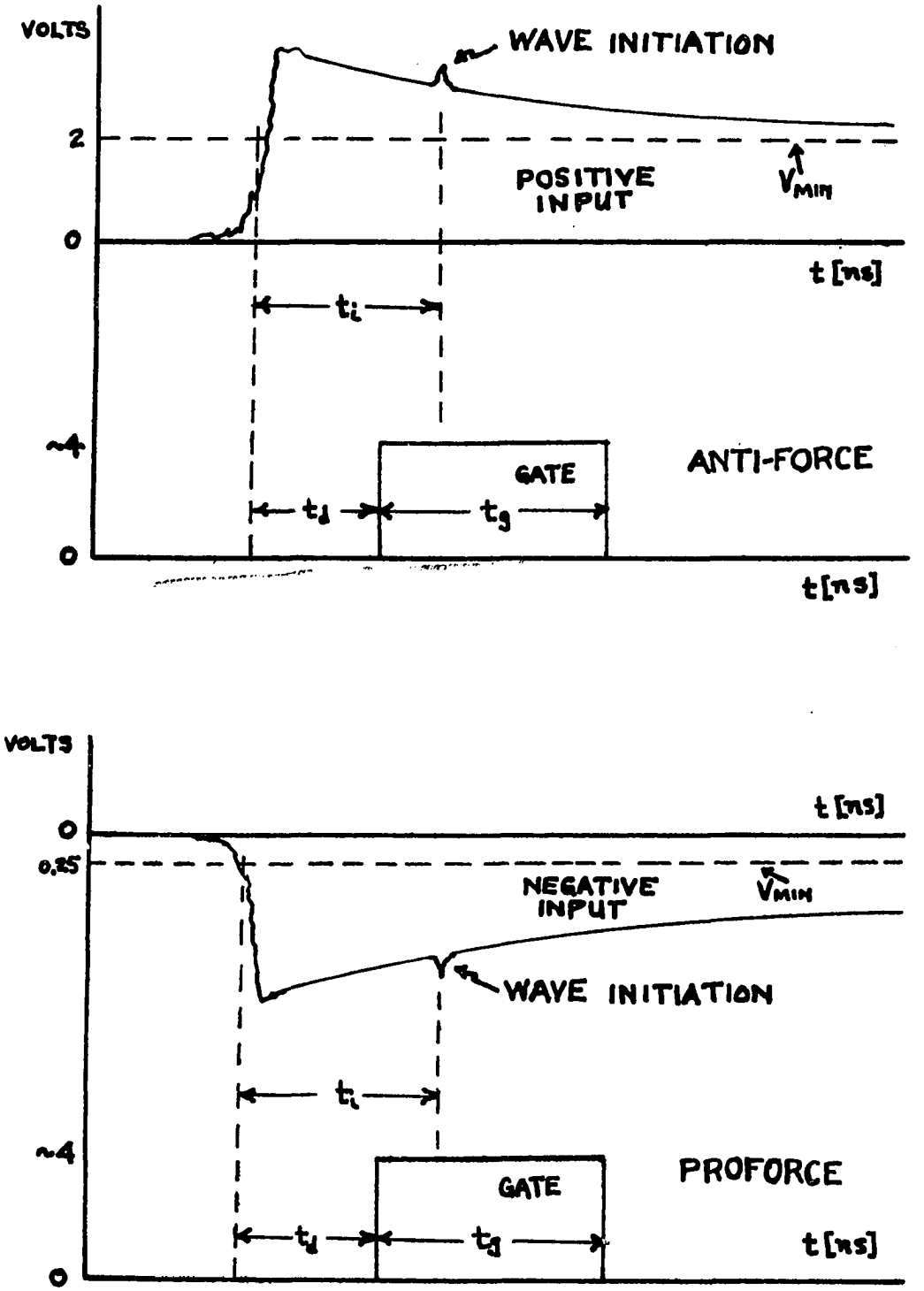

Voltage scale grossly exaggerated. ΔV less than 0.5% during t_g.

Figure 7. Delay gate pulse.

data on the anti-force case. Now the variation in initiation time t_i causes a significant variation in applied voltage if t_i is on the order of t_{RC}, the natural time constant of the main capacitor and the driver resistors. Calculation and observation lead to the same value for t_{RC}, 750 μs. Thus, a variation of 100 μs in t_i leads to a voltage drop of 12 per cent. Of course the wave speed is variable.

The DGG was used in the following procedure. A signal was taken from the 6000 to 1 resistive voltage divider on the breakdown tube. The signal was applied to either the positive or negative input of the DGG. Thus, an anti-force (positive electrode) wave of 12 kV or a proforce wave of 1.5 kV is capable of initiating DGG operations. After a preselected time t_d the gate is on for t_g. Unless a light pulse from the start viewport can make the journey to the TPHC and arrive during t_g no output pulse will result. Therefore, there exists a time window that corresponds to an applied tube voltage window, and only those waves initiated in the window are good enough to count. Now, even if the largest temporal window were used, 4 μs, then the voltage variation must be less than one half of one per cent. The DGG, of course, slows down the data acquisition rate and frequently necessitated running the tube for more than one hour with a PRF of one pulse per second to gain a single datum. Consistency, nonetheless, outweighs convenience.

Wave speed procedure. The determination of times of flight was made not by calibrating each component of the system, but by calibrating the system as a whole from TPHC to MCA. One needs merely to know that a given channel corresponds to a given time when using range r on the TPHC. One measures several points and determines a rule for interpolation

to take channel number into time. For a system so linear the rule is not hard to find.

Calibration was carried out by applying one of two types of known time delay to the system. With either delay the signal from a Tektronix type 105 square wave generator was fed through a differentiator and clipping circuit to a BNC T connector. The connector applied the signal, now a negative spike, to both the start input of the TPHC and to the known delay. The delay led to the stop input. Two devices were used for this purpose, a delay amplifier and a set of delay lines. The delay lines were considered more accurate and were used for all ranges up to 1 μs. The delay amplifier was calibrated against the lines and then used to extend the calibration out to the next order of magnitude.

Whichever device was used the system was calibrated one TPHC range at a time, by using each member of a set of delay times that fell within the selected range. Due to linearity only two points were needed, but all were done. All counts from a single delay would generally fall into a single channel, though occasional overlap occured. This method of doing a single channel at a time was found to be more accurate than using a single delay and switching ranges. This was probably due to switching transients. Originally the calibration curves were plotted from a least squares fit to a linear equation. A simpler graphic method was well within the bounds of experimental error. Normally a weekly calibration was performed. At the beginning and end of each data run one or two points on one or two ranges were replotted to make

certain that no one had accidentally turned any knobs. The stability of the system was such that none of these checks ever necessitated a recalibration. To insure stability the system was allowed to run constantly even between data taking periods.

The delays. The delay lines were described by Gary E. Copeland in his 1970 dissertation.[18] They were 50Ω RG 58/U cable with a standard BNC connection at each end. They were calibrated by feeding a pure sine wave into one end via a T connected to a null detector. The signal at the cable's other end also went into the detector. The signal at the far end of the cable is phase shifted due to the delay t_d. For a null t_d must correspond phase shift of π. By sweeping frequencies one learns what t_d is since it must be the reciprocal of the frequency differences between successive nulls. With a Tektronix 190B constant amplitude signal generator sweeping from 1 to 50 MHz, a Hewlett-Packard model 524D frequency counter and a 525A frequency converter Copeland measured the lines and found values of: 28.0±0.3, 44.0±0.02, 88.09±0.90, 88.7±0.77, 101.4±0.50, 183.2±1.6, and 378.5±2.2 all measured in nanoseconds.

The delay amplifier was an ORTEC 427A module with a range of delays from one quarter microsecond to 4.75 microseconds by quarter microsecond increments. By calibrating the amplifier against the delay lines a correction was made. Its linearity was good and it could be used to extend the range of measurement up to ten microseconds.

Temperature and Density Diagnostics

The method used for determining electron temperatures and densities is a spectroscopic method based on the ratio of intensities of two helium emission lines. Refinements in them and its application to a similar problem were reported by Latimer, Mills and Day[19], and a more extensive review of the theory involved was made by Bićanić[20], though he applied the method to argon.

A Jarrell-Ash quarter meter monochromator was used with a 0.20 mm inlet slit and a 0.28 mm out slit. Mounted at the out slit was the same 7746 PM described above. The signal was sent to a Tektronix 519 oscilloscope, an instrument with a fixed vertical sensitivity of 9.4 volts/cm and a remarkable measured rise time of 0.28 nanosecond.

In operation the monochromator was positioned at one of three positions 2.0 m, 3.5 m, or 5.0 m from the discharge electrode. These ports were free from light pipes and the instrument could be positioned accurately with its inlet slit a distance of 17.0 cm from the center of the discharge tube and 14.5 cm from the closest point of the pyrex tube at the 0.5 cm wide slot. The monochromator was then clamped into position. A trigger signal for initiating the scope sweep was provided by the 8475 PM mounted at the 1.75 m position. Using an external trigger assured at least three bits of z versus t data by measuring the time delay before onset of the wave at the three positions. Thus, one could be certain that if questions were later asked of the speed of this wave, one could check its agreement with the preceding work.

Results were preserved by a Polaroid camera mounted on the scope face. One measurement was recorded at each of the two wavelengths,

λ = 4713 Å and λ = 5048 Å, on the same piece of film.

Calibration was made against a standard lamp using the method described by St. John[21]. The intensity ratios yield the electron temperatures while the absolute intensity yield the densities.

CHAPTER III

WAVE SPEED ANALYSIS

As described above, wave speeds were recorded as a series of time intervals required for the wave to travel the distance between a trigger station at 1.75 m from the electrode and a stop station at (z-1.75) meters farther down the tube. These were then plotted as a z versus t curve as shown by Graph A, a typical data graph at the top of Fig. 8. Approximate velocities were then estimated by looking at $\Delta z/\Delta t$ for finite intervals at each value of z down the tube. A plot was made of $\Delta z/\Delta t$ versus z on semilog paper with the z value on the linear scale. An example of this plot appears at the bottom of Fig. 8. With the exception noted below this approximate velocity graph appears to have a negative linear slope. We might therefore assume that v follows an exponential decay curve. Then we can make a corresponding correction on the graph plotted above. Extrapolating the corrected line back to the electrode at z equals zero yields a value for v_o.

We can tell from our z vs t graph that the time difference between z_2 and z_1 is equal to t_2-t_1. It is important to calculate the instantaneous velocity at z from the known data for finite intervals. If we assume the form

$$v = v_o e^{-\alpha z}$$

then we can calculate a correction factor for changing $\Delta z/\Delta t$ into

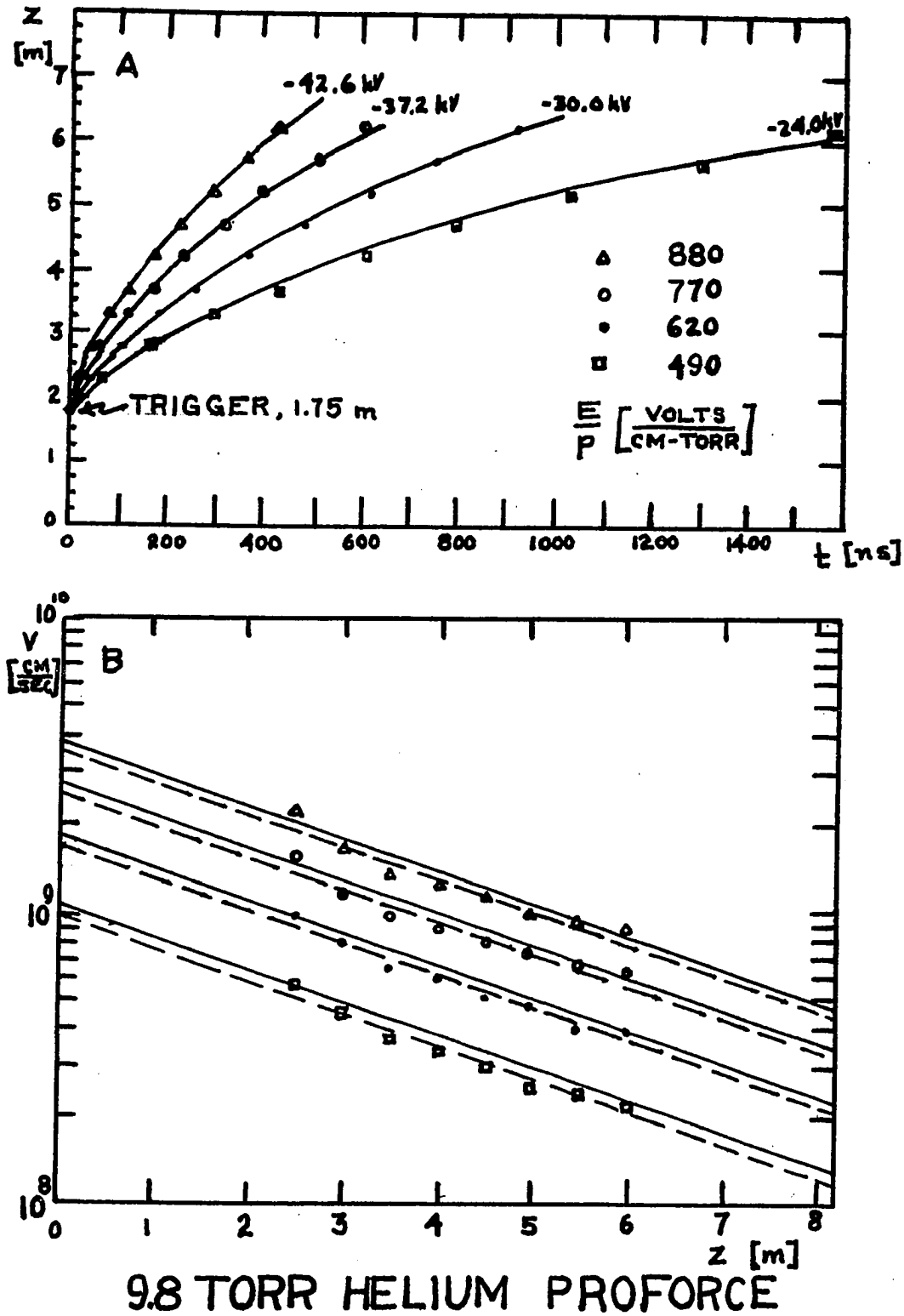

Figure 8. z versus t and v versus z.

$dz/dt = v$. One can choose α from the experimental data in Graph B.

Let us assume not only that the equation above is true, but also that its being an equation based on nature guarantees that appropriate boundary and continuity conditions hold then

$$\frac{1}{v} = \frac{dt}{dz} = \frac{e^{\alpha z}}{v_o} \quad .$$

Therefore, we can calculate all higher order derivatives of t with respect to z. These are

$$\frac{d^2t}{dz^2} = \frac{\alpha e^{\alpha z}}{v_o} \quad , \quad \frac{d^3t}{dz^3} = \frac{\alpha^2 e^{\alpha z}}{v_o} \quad , \quad \ldots, \quad \frac{d^nt}{dz^2} = \alpha^{(n-1)} \frac{e^{\alpha z}}{v_o} \quad .$$

Knowing these we can expand t as a Taylor series about $z = z_1$.

$$t_2 = t_1 + \left(\frac{dt}{dz}\right)_{z=z_1} (\Delta z) + \frac{1}{2!}\left(\frac{d^2t}{dz^2}\right)_{z=z_1} (\Delta z)^2 + \cdots$$

where $\Delta z = z_2 - z_1$. Thus,

$$\Delta t = t_2 - t_1 = \frac{e^{\alpha z} \Delta z}{v_o} \left[1 + \frac{\alpha}{2}(\Delta z) + \frac{\alpha^2}{6}(\Delta z)^2 + \cdots\right] .$$

Now $\frac{e^{\alpha z}}{v_o}$ is simply $\frac{1}{v}$ @ z_1, so multiplying through by $\frac{v(z_1)}{\Delta t}$ we find

$$v(z_1) = \frac{\Delta z}{\Delta t} \left[1 + \frac{\alpha}{z}(\Delta z) + \frac{\alpha^2}{6}(\Delta z)^2 + \cdots\right] .$$

Now multiplying by $1 = \frac{\alpha \Delta z}{\alpha \Delta z}$

$$v(z_1) = \frac{\Delta z}{\Delta t} \frac{\left[\alpha \Delta z + \frac{\alpha^2}{2} (\Delta z)^2 + \frac{\alpha^3}{6} (\Delta z)^2 + \cdots\right]}{\alpha \Delta z} \quad .$$

Inside the brackets add $0 = 1 - 1$.

$$v(z_1) = \frac{\Delta z}{\Delta t} \frac{[1+\alpha\Delta z+ \frac{\alpha^2}{2} (\Delta z)^2+ \cdots -1]}{\alpha\Delta z}$$

$$= \frac{\Delta z}{\Delta t} \frac{[e^{\alpha\Delta z}-1]}{\alpha\Delta z}$$

$$= \frac{e^{\alpha\Delta z}-1}{\alpha\Delta t} \quad .$$

Since each measurement was made over a 50 cm distance from its previous value one finds that Δz is fixed and we can thus define a quantity

$$L = \frac{[e^{\alpha\Delta z}-1]}{\alpha} \quad ,$$

which is a constant for any given value. L is the effective distance interval. Therefore, the refined value for velocity is

$$v(z_1) = \frac{L}{t_2-t_1} \quad .$$

Figures 8, 9 and 10 show examples of the calculation in graphic form.

By extrapolating the corrected line back to z = 0 we can assign to any given pressure and tube voltage a single number, v_o. By plotting this versus E/p we can directly compare the measured values with Shelton's theory.

Computing the Electric Field

This brings one to the point of deciding what electric field is operating in the tube. This problem was approached in two different ways by Dr. R. G. Fowler, who used an experimental method and Dr. S. E. Babb, Jr., who solved Poisson's equation for the boundary conditions of a half infinite pair of concentric cylinders. The geometry is diagrammed below.

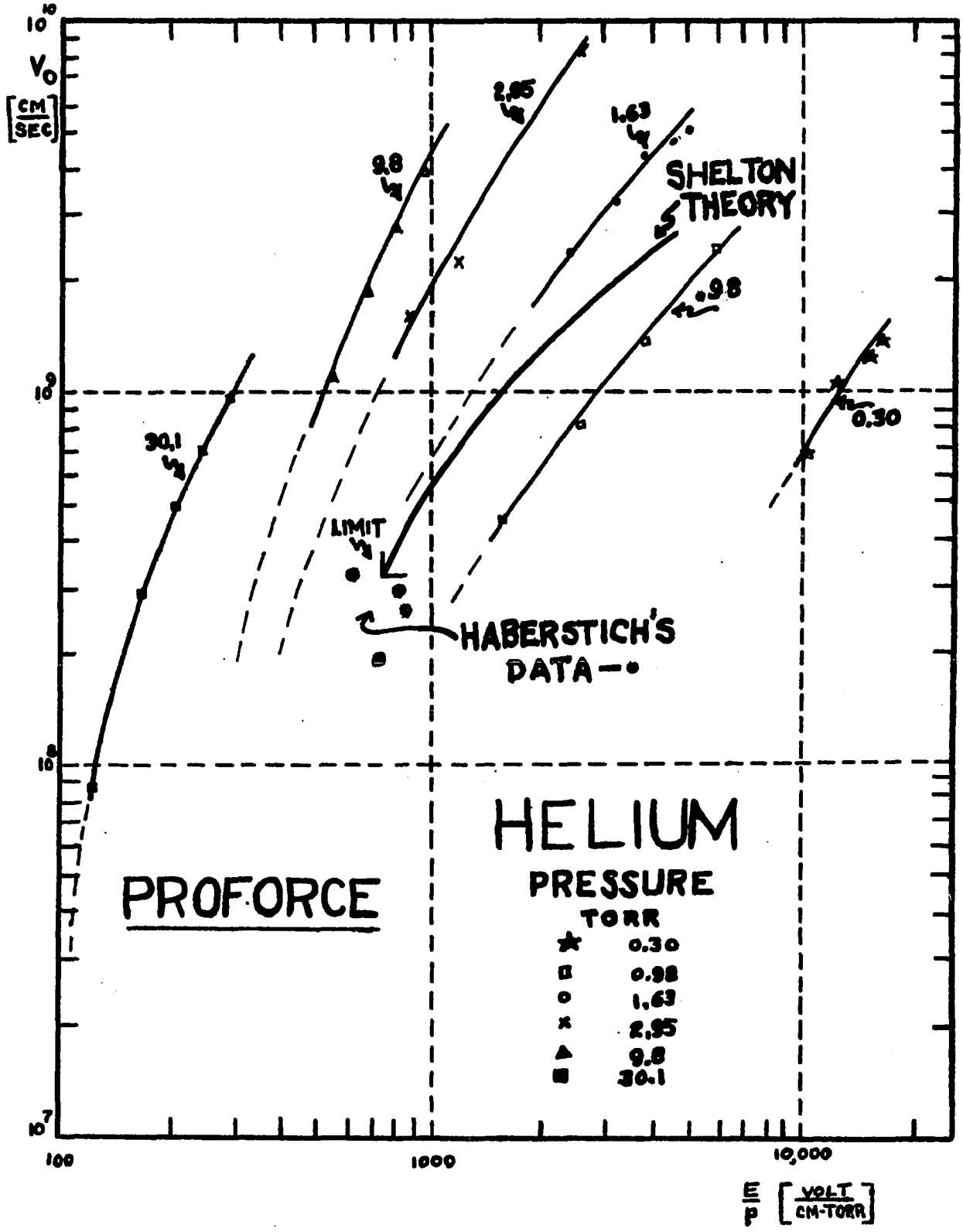

Figure 9. v versus $\frac{E}{p}$, proforce.

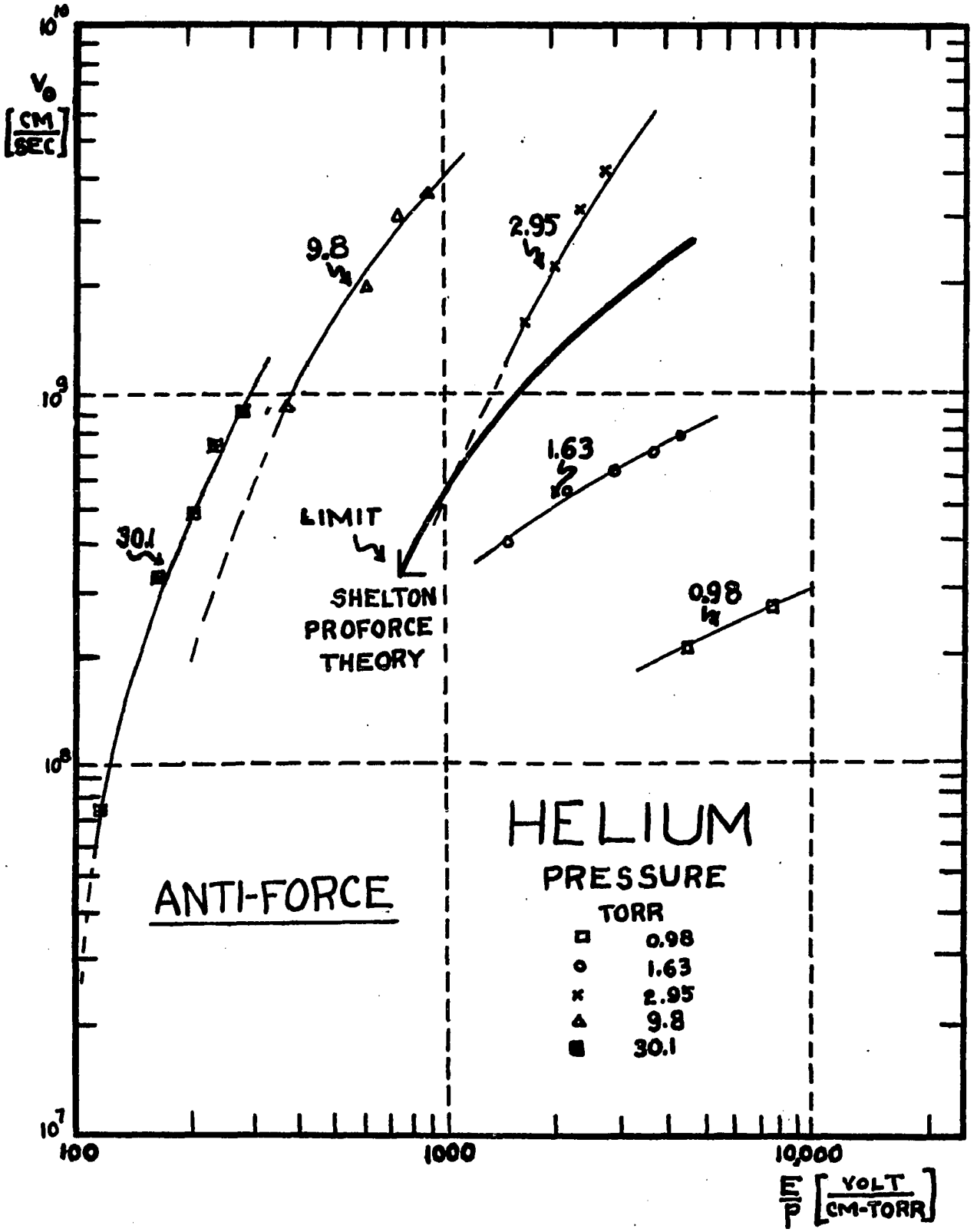

Figure 10. v versus E/p, antiforce.

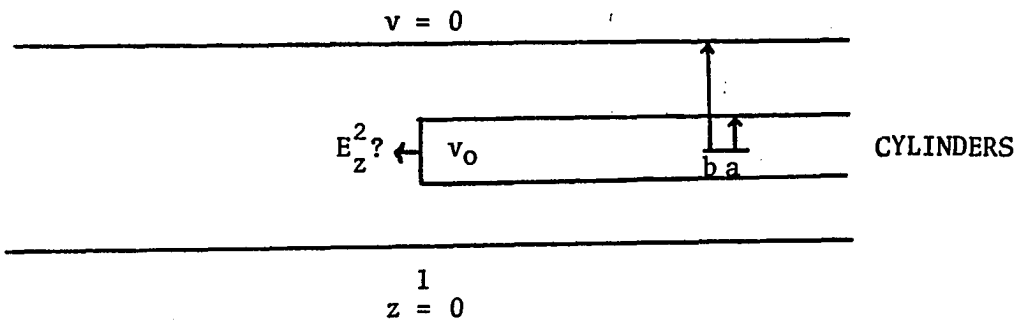

Fowler's method was to set up an electrolytic tank and actually probe the potential as a function of z along the axis. His result was

$$E = \frac{0.555}{a} v = 0.222v \ .$$

Babb's method was to solve Poisson's equation with appropriate boundary conditions for this semi-infinite geometry. To accomplish this he first broke the space into three regions, one to the left of the z = 0 plane, a second to the right of the z = 0 plane and with r < a, and a third to the right of z = 0 but with b>r>a. He then matched boundary conditions across the appropriate interfaces. After a great deal of manipulation an iterative solution compatible with computer evaluation was found. The solution can be plotted in the whole space, but the only point of interest to us is at z = 0, r = 0. Babb's result is

$$E = \frac{0.507}{a} v = 0.203v \ .$$

This value differs from Fowler's experimental value by less than ten per cent.

While these results agree there are several dubious points that remain. First those values are for a right circular cylinder with sharp edges at $z = 0$, $r = a$. The actual wave undoubtedly has an added degree of freedom typical of a fluid phenomenon. It can select a shape for its wavefront different from a simple plane defined by $z = 0$, $r \leq a$. This shape could be modified by viscous forces at the walls, charge distribution, or a variety of causes that the one dimensional Shelton theory never examined.

A second influence that calls the validity of the field expressions above into question is the effect of the dielectric tube wall. If one considers two infinitely long coaxial conducting cylinders of radii a and b and then calculates the radial field between them, he finds that slipping a pyrex pipe like ours over the inner conductor alters the field by a factor of four.

Both of the above influences being debatable, it is likely that the symmetry of evaluating E_z on the z axis diminishes any deleterious effect they might contribute. Furthermore, we can certainly try the above expressions for comparison of experiment to theory, for we have no better approximation to work with. The following wave speed versus field calculation shall be based upon Babb's value on the theory that Fowler's value gives excellent physical confirmation to Babb's result, but may contain experimental errors of greater magnitude than the numerical errors in Babb's expression.

Comparison to Theory

Having now found the wave speeds and the electric field, we can plot the former versus the latter and look at Fig. 9 and Fig. 10. The prediction of the Shelton theory is shown on the graphs together with the data. Mainly three things require comment; the pressure dependence, the differing results for proforce and anti-force waves, and the nature of the low velocity cut-off.

The curve plotted to represent the Shelton theory is plotted to a normalized scale of pressure one Torr. Yet no pressure dependence is predicted by the theory. It is clear from the data that pressure is indeed a very important parameter. The pressure dependence seems to have the following characteristics. As pressures rise the two types of waves behave increasingly alike to the extent that by 30 Torr they look identical. As pressure drops the proforce wave keeps at least the form of the theoretical curve, but the anti-force wave entirely goes to pieces. At 0.30 Torr the statistics are so bad that no meaningful data can be extracted on the anti-force case.

In addition the pressure dependence that does occur bears a strong resemblance to the Paschen curve. For a given field strength there is a pressure at which maximum speed occurs. The maximum for helium is apparently between one and two Torr. The physical explanation seems to be that at high pressures the mean free path of electrons is so short that it cannot gain sufficient energy from the electric field between collisions to produce ionization, while at low pressures the mean free path becomes comparable with apparatus dimensions causing the

inelastic electron collisions to become an inefficient ionization mechanism. The above result is in perfect agreement with Haberstich.

The anti-force wave seems to go to pieces at low pressures and become extremely random. At first it was thought that this might be due to a stepped leader phenomenon which an observation method using only two viewports fails to detect. It is well known that lightning exhibits a stepped leader nature, which is to say it proceeds by fits and starts racing along at high speed for several tens of meters, halting for a fraction of a second, then racing off once again. In this writer's knowledge this has never been seen in controlled laboratory conditions, nor has the theory of its governing mechanism been adequately described. If such a phenomenon occurred in the discharge tube, obviously the statistical data taking method combined with merely two viewports would mask its nature. To observe such a phenomenon multiple observation of a single discharge would be required. A system of mirrors and lenses was jury-rigged to test six viewports simultaneously with two photomultipliers and a Tektronix 555 dual beam oscilloscope. A null result was discovered for on any given firing a single wave was observed, but its actual speed was random. One can only speculate on the cause for this, as will be done in the following chapter.

Finally, with regard to the low velocity cut-off predicted by Shelton, there is definite evidence that such a cut-off exists. It is difficult, however to determine its precise value. As the field is lowered toward the cut-off value the wave initiates only intermittently This is probably due to the lack of electrons in the vicinity of the

electrode. If the wave is ever capable of propagating then presumably you are not below cut-off. The criterion for declaring oneself below the Shelton cut-off was that no wave was optically observed in one hundred electrode pulses. The cut-off being sketchy, and the low voltage end of each curve being also less well known due to increased randomness of speed on each firing, the v versus $\frac{E}{p}$ graphs were drawn with the lower end dotted indicating a section in which the curve may or may not be significant.

One final feature is of interest from the wave speed results. The exponential decay constant α appears tc be a constant as a function of pressure. One finds α equals $0.290 \pm 0.004 (\text{meters})^{-1}$. Even for the case at 0.30 Torr which at first sight appears to have no decrement, one finds that an α as above is consistent with the error bars. The exponential decay was not recognized by Haberstich owing to the manner in which he expressed his data. Moreover, when values were taken from his data they seemed to be pressure dependent. Due to our improved measuring technique, the greater abundance of our data, and our undoubtedly superior gas purity, the freedom of α from pressure dependence seems to be established. Pressure independence suggests that α is related to equipment parameters such as the radius or length of the ground array rather than to a property of the gas itself.

The data presented in figures 9 and 10 is obviously in a highly condensed form. The dubious nature of the electric field calculation has already been mentioned. Mention has further been made that the v_o evaluation is somewhat arbitrary. It may be that effects at the driver

end associated with wave formation are strongly pressure dependent. The point at which the exponential decay becomes physically meaningful might be a $z_o=z_o(p)\neq 0$. Thus, by arbitrarily extrapolating all data to $z_o=0$ we may have artificially introduced a pressure dependence into Sheltons data that does not exist in nature. Consequently, it seemed best to present the raw data for z versus t upon which the graphs were based, so that if future work suggests a better form for analysis than the one employed here, the value of the data will not be likewise diminished. This data is included in tabular form in Appendix B.

Wave Temperature Results

The method for determining electron temperatures has been described by Latimer, Mills and Day as noted above, and a fuller bibliography is available in Bićanić. The method attempted here differs from these others in that it applies to a time varying case rather than to a steady state. The essential idea is this.

An atom in an excited state i can decay to a lower state j by release of a photon of energy $h\nu_{ij}$, where h is Planck's constant and ν_{ij} is the frequency associated with the i to j transition. The steady state light intensity at that frequency produced by a unit volume of gas at density N_o will be $J_{ij}=A_{ij}n_i h\nu_{ij}$ where A_{ij} is the transition probability and n_i is the number of atoms in the upper excited state. The PM sees photons, so consequently the current measured at the PM output will be $I_{ij}=f_{ij}\frac{J_{ij}}{h\nu_{ij}}$ where f_{ij} is a constant depending on the spectral response of the phototube and the optical parameters of the system.

For the non-steady state one finds that $\frac{dI_{ij}}{dt} = -A_{ij}I_{ij} + p(T_e)$ where $p(T_e)$ in these unusual units is a function of the electron temperature, the number density of electrons, and the constant f_{ij}. This picture assumes that excitation is primarily by electron collision, with cascade effects, etc. negligible. By transposing the first term on the right and dividing the above equation by a similar one for a different transition, such as the m to n transition, a ratio can be found of $p_{ij}(T_e)$ to $p_{mn}(T_e)$ experimentally. Provided the functional dependence of the two p's on T_e is different, such as would be typical in comparing a singlet to a triplet transition, one finds that the ratio of the p's and therefore of the left members, is a function of the electron temperature. The ratio of the p's has been tabulated in Latimer, Mills and Day for the 5048°A transition and the 4713 ^{o}A helium transition. In sum, one experimentally measures the left member of

$$\frac{\frac{1}{f_{ij}A_{ij}}\frac{dI_{ij}}{dt} + I_{ij}}{\frac{1}{f_{mn}A_{mn}}\frac{dI_{mn}}{dt} + I_{mn}} = \frac{p_{ij}(T_e)}{p_{mn}(T_e)}$$

and then compares it to the tabulated values of Latimer, Mills and Day. The I's can be experimentally measured in arbitrary length units of an oscillograph. Such scope photos were enlarged with an opaque projector onto graph paper, a smooth curve was drawn to fit them and values were read off at ten nanosecond intervals. The ratio on the left was then computed on an IBM 1130.

The raw data fed to the computer for a series of measurements made at 2.95 Torr are given in Appendix C. Code numbers are read as fol-

lows. The three digits represent the applied electrode voltage for the test times ten. A, B, and C represent antiforce waves, while D, E, and F designate proforce. A and D were measured at z = 2.0 m, B and E at = 3.5m and C and F at z = 5.0 m. Therefore, 360 C signifies a wave of 36.0 kV electrode potential, antiforce polarity and measured at 5.0 m from the electrode. Data is presented in rows with 5048 data preceeding 4713. The numbers along the row give thirty I_{ij} values at ten nanosecond intervals, two rows being used for a given line.

The results of the measurements are not conclusive, but they do suggest some goals for further research and they do display the difficulty of wave structure studies. The rapid time scale of the wave as predicted by Shelton implies that the wave will be well beyond the thin sheath of high temperature by the time our first data point is resolved at ten nanoseconds. His prediction of 100 eV electrons for a wave at $10^9 \frac{cm}{sec}$ is much larger than we can resolve. Our values, at from 10 eV to 15 eV are more in keeping with the quasi-neutral region behind the wave front. In addition, computer analysis is perhaps more misleading than helpful. The values of T_e will also be quite sensitive to pressure dependence of the lifetimes. It does seem valid to draw two generalizations from the temperature data. Antiforce waves show more structure than proforce and are probably hotter. The light intensity output is consistent with a short square pulse of hot electrons providing excitation. Figure 11 illustrates this.

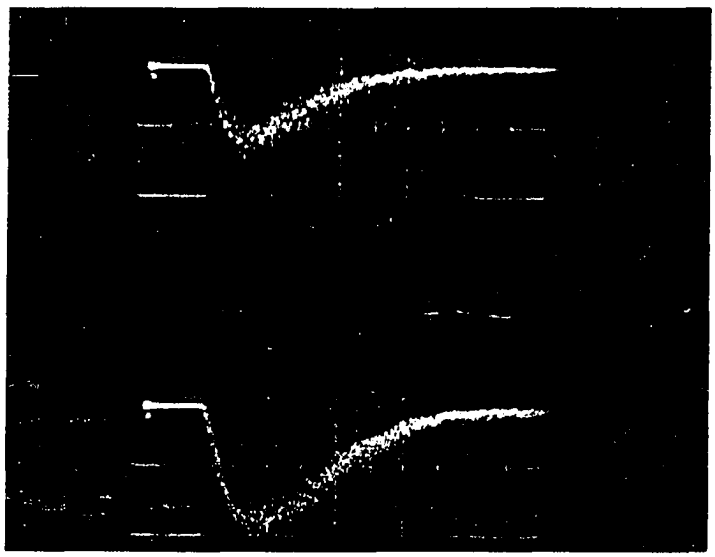

(a) Proforce 42.0 Kv wave 5 m from electrode 100 ns/cm: horizontal. Top trace, λ = 5048Å; Bottom, λ = 4713Å. Time delay from trigger to onset artifically differs from below.

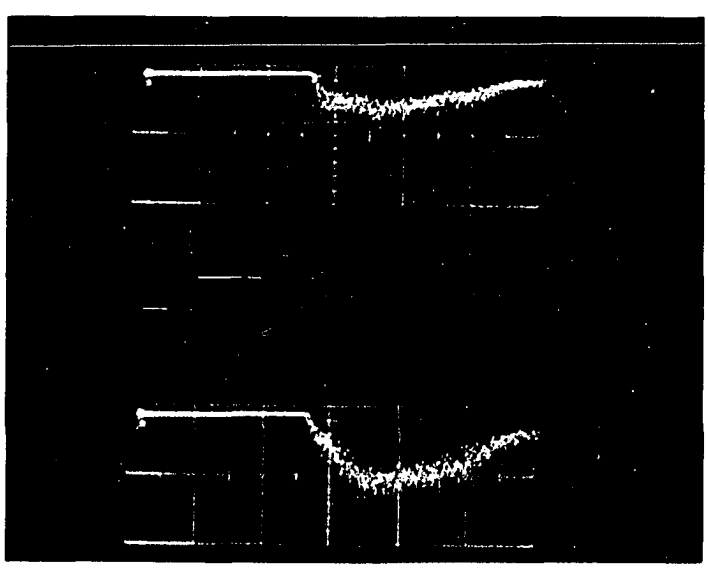

(b) Antiforce 42.0 kV wave 5 m from electrode 100 ns/cm: horizontal. Top trace, λ = 5048 Å, Bottom, λ = 4713 Å.

Figure 11. Antiforce versus proforce.

Filmed as received

without page(s) 53 .

UNIVERSITY MICROFILMS.

CHAPTER IV

CONCLUSIONS AND SPECULATIONS

It is possible to offer a qualitative explanation for some of the discrepancies between the observed wave speeds and the Shelton theory. Undoubtedly the most salient distinction is that the theory is one dimensional while the wave in the physical tube is obviously three dimensional. If in fact the wave does not have a plane shock profile then the radial parameters might introduce an adjustable variable that is highly pressure dependent. In viscous flow through a pipe it is classically known that the velocity profile as a function of radius is a parabolic distribution with maximum velocity at the tube center. The actual face of the wave might be similar to this classic phenomenon, Poisieulle flow, with the face shape being strongly pressure dependent at pressures near one Torr.

Another qualitative explanation that would explain the peculiar kink in the data, in which at a certain point down the tube the exponential velocity decay with distance ceases and the wave becomes a constant speed wave. The phenomenon is only noticeable in the proforce wave. By looking at the data in Fig. 8b, one notices that while an exponential decay law for wave speed with distance appears to approximate the data, there is a tendency for the e folding distance to increase after a certain point down the tube. In fact, with some of the data,

the wave appears to go off with a constant velocity after it reaches a certain point along the tube. This constant velocity is lower than the velocity at the Shelton limit.

One might speculate that if speed, v, is proportional to $e^{-\alpha z}$ where α is the reciprocal of the e folding distance, then E, the electric field at the front, which satisfies a form according to Shelton of

$$v = AE - \frac{B}{E}$$

must also have a decrement proportional to $e^{-2\alpha z}$. This would generate a point z_0 down the tube at which E would diminish to the Shelton limit. The wave at this point would stall out with the unstable situation existing in the tube of one region of the tube ionized and with a high voltage at one end of it, and the other region of the tube unionized. But field decrement across the plasma implies a voltage drop from electrode to stalled wave front. Since the electrode stays at high voltage longer than the recombination time of the ions, and since the plasma is a good conductor, the wave front will tend to rise in voltage to equilibrate the plasma. As the field again climbs to the Shelton limit the front can move ahead a few centimeters returning to the stalled condition. This all occurs as a smooth process. Thus, the Shelton limit determines the point at which the wave stalls out and begins to move at a constant speed, but the parameters of the plasma behind the wave front determine that speed of propagation beyond this point. After this point the speed is less determinate, as one would typically expect with waves initiated at the Shelton limit.

The verification of this is complicated by not knowing exactly the value of the Shelton limit as a function of pressure and by the increased randomness mentioned above. Also, after this point is reached, the runs are not long enough to substantiate this exactly. Also, without a longer tube, the point at which one draws the break in the v versus z data is somewhat arbitrary. The question must be left to future investigation.

The above remarks are at best speculation. It is proper, however, to note here what firm conclusions can be drawn from the experiments conducted. First, the claim that the wave speed data presented above is superior to any previously available could be substantiated by noting that the technique was an improvement both in calibration and in statistical acquisition, the gas was more pure, the pressure regime extended from one third of the pressure previously measured to four times higher than investigated before, the field range doubled Haberstich's and that data was acquired at many more points down the tube. An immediate conclusion is that the functional form of the Shelton predicted velocity - field relation is not bad, but that the evaluation of its absolute magnitude will require further investigation and consideration. The velocity decrement observed in a Haberstich tube is most likely a function of the apparatus geometry. The temperature structure of the wave front is not clearly revealed by the time resolved line intensity technique because of the extremely short duration predicted by Shelton.

BIBLIOGRAPHY

1. F. Hauksbee, Philosophical Transactions of the Royal Society *XXV* (Issue 307), 2277-2282 (1706).

2. C. Wheatstone, Pogg. Ann. *34*, 148 (1835).

3. W. von Zahn, Pogg. Ann. *8*, 675 (1879).

4. J. J. Thomson, *Recent Researches* (Oxford University Press, New York, 1893), p. 115.

5. J. W. Beams, Phys. Rev. *36*, 997 (1930).

6. L. B. Snoddy, J. W. Beams and J. R. Dietrich, Phys. Rev. *50*, 469 (1936).

7. L. B. Snoddy, J. W. Beams and J. R. Dietrich, Phys. Rev. *52*, 739 (1937).

8. F. H. Mitchell and L. B. Snoddy, Phys. Rev. *72*, 1202 (1947).

9. B.F.J. Schonland, in *Encyclopedia of Physics*, edited by S. Flugge (Springer-Verlag, Berlin, 1956), Vol. 22, p. 576 ff.

10. B.F.J. Schonland, Proc. Roy. Soc. (London) *A164*, 132 (1938).

11. L. B. Loeb, Science *148*, 1417 (1965).

12. R. A. Nelson, Phys. of Fluids *8*, 23 (1965).

13. R. G. Fowler and J. D. Hood, Jr., Phys. Rev. *128*, 991 (1962).

14. G. W. Paxton and R. G. Fowler, Phys. Rev. *128*, 993 (1962).

15. A. Haberstich, "Experimental and Theoretical Study of An Ionizing Potential Wave in A Discharge Tube," Ph.D. Dissertation, University of Maryland (1964).

16. G. A. Shelton, "An Investigation into the Structure of Electron Fluid-Dynamical Waves." Ph.D. Dissertation, University of Oklahoma (1967).

17. R.W.P. King, *Transmission Line Theory*. (New York: Dover Publications, Inc., 1965).

18. G. E. Copeland, "Lifetimes of Excited Electronic States of Chemically Active Gases." Ph.D. Dissertation, University of Oklahoma (1970).

19. I. D. Latimer, J. I. Mills and R. A. Day, J. Quant. Spectrosc. Radiat. Transfer *10*, 629 (1970).

20. D. D. Bicanic, "Spectroscopic Measurement of the Electron Temperature in the Tenuous Argon Ion Laser Plasma." M.S. Thesis, Old Dominion University (1971).

21. R. M. St. John, Meth. Exper. Phys. *8*, 27 (1969).

APPENDIX

THE SHELTON THEORY

The Shelton theory analyzes breakdown waves in a frame of references traveling with the wave front in which a solution is sought in the form of a steady profile wave for the fluid-dynamical equations of conservation of mass, momentum and energy of a three fluid system. The three fluids are composed of the electrons, the positive ions and the heavy neutrals. The initial one dimensional geometry assumed envisions an infinite slab of electrons confined between x and x + dx immersed in an infinite sea of neutral particles and experiencing a uniform electric field pointing in the negative x direction and of sufficient strength to accelerate electrons to energies appropriate for collision ionization in the time between collisions. For this one dimensional model in every portion of the geometry ionization must replace electrons lost by flowing away.

Shelton uses lower case letters to designate electron quantities, unsubscripted upper case letters to signify heavy neutral particle quantities and upper case letters subscripted with i to symbolize positive ion quantities. As an example this rule would state that n (N,N_i) symbolizes electron (neutral, positive ion) number density, m for particle mass and V for velocity. Partial pressure of electrons is p_e with corresponding P and P_i and with T_e as electron temperature.

Because heavy species naturally interact strongly and because our attention is focused on the electrons, he sets both of the heavy particle's speeds equal to $V = V = V_i$. The heavy particle pressure will be designated as $P_h = P + P_i$. The electric field will be designated by E, the ionization frequency by β, the elastic collision transfer term for momentum [energy] by $\Delta_c(mv)$ $[\Delta_c(\frac{1}{2}mv^2)]$, and the corresponding inelastic quantity by Δ_i^s. The superscript s designates the species with e for electrons and h for either heavy particle. Interest in distinguishing between heavy species is further suppressed by combining the ion and neutral equations for both momentum and energy. Since the waves are steady profile the time derivatives of all quantities in the wave frame will equal zero and the one dimensional nature of the system will allow the replacement of divergences, etc. in the fluid-dynamical equations with total derivatives with respect to x. Due to the appearance of the same constant mass in all terms of the continuity (mass conservation) equations, mass can be cancelled out, implying the obvious fact that mass conservation is identical to particle number conservation. The species equations then become

$$\frac{d}{dx}(nv) = \beta n \tag{1a}$$

$$\frac{d}{dx}(N_i V) = \beta n \tag{1b}$$

$$\frac{d}{dx}(NV) = -\beta n \tag{1c}$$

$$\frac{d}{dx}(mnv^2+p_e) = -enE - \Delta_c(mv) + \Delta_i^e(mv) \tag{2a}$$

$$\frac{d}{dx}(MNV^2+M_iN_iV_i^2+P_h) = eN_iE + \Delta_c(mv) - \Delta_i^h(mv) \tag{2b}$$

$$\frac{d}{dx}\left[\tfrac{1}{2}mnv^3-(p_e-q)v\right] = - envE - \Delta_c(\tfrac{1}{2}mv^2) + \Delta_i^e(\tfrac{1}{2}mv^2) \qquad (3a)$$

$$\frac{d}{dx}\left[\tfrac{1}{2}MNV^3+\tfrac{1}{2}M_iN_iV^3+(P_h+Q)V\right]= eN_iVE + \Delta_c(\tfrac{1}{2}mv^2) - \Delta_i^h(\tfrac{1}{2}mv^2) \ . \qquad (3b)$$

Shelton next examines whether currents exist in the wave. Writing the complete electron and positive ion continuity equations including source terms and time derivatives

$$\frac{\partial n}{\partial t} + \frac{\partial}{\partial x}(nv) = \beta n \qquad (4a)$$

$$\frac{\partial N_i}{\partial t} + \frac{\partial}{\partial x}(N_iV) = \beta n \qquad (4b)$$

He subtracts Eq. (4a) from Eq. (4b) and multiplies the result by e yielding

$$\frac{\partial}{\partial t}\left[e(N_i-n)\right] + \frac{\partial}{\partial x}\left[e(N_iV-nv)\right] = 0 \ .$$

Knowing Poisson's equation

$$\varepsilon_o \frac{dE}{dx} = e(N_i-n) \ , \qquad (5)$$

a simple substitution with interchange of derivatives leads to

$$\frac{\partial}{\partial x}\left[\varepsilon_o \frac{\partial E}{\partial t} + e(N_iV-nv)\right] = 0 \ .$$

Integration yields

$$\varepsilon_o \frac{\partial E}{\partial t} + e(N_iV-nv) = i_o(t) \ .$$

The portion of the gas which is as yet free from ions can of course contain no convective currents. The one dimensional geometry guarantees that the field is constant in that region also, so that no displacement

current exists there. Therefore, $i_o(t) = 0$ and obviously

$$\varepsilon_o \frac{\partial E}{\partial t} + e(N_i V - nv) = 0 \quad .$$

For a steady profile wave the time derivative of field is, of course, zero. Thus, it is established that

$$N_i V - nv = 0 \quad .$$

This says that if one is in the wave frame a zero current condition must hold. With no currents, no external magnetic fields and no time derivatives in the wave frame it becomes apparent that Maxwell's equations reduce entirely to Eq. (5), Poisson's equation.

Shelton next examines the form of the elastic transfer operators. By averaging over all impact parameters with an assumed Maxwellian speed distribution and an empirical inverse speed cross-section he calculates the elastic electron momentum transfer operator in the rest frame of the heavy particles as

$$\Delta_c^o(mv) = \frac{4}{3} \sigma_o V_o N m n (v-V) \simeq K_1 m n (v-V)$$

where the superscript ^{o} indicates the rest frame. In an arbitrary frame

$$\Delta_c(mv) = \Delta_c^o(mv)$$

and

$$\Delta_c(\tfrac{1}{2}mv^2) = V\Delta_c(mv) + \Delta_c^o(\tfrac{1}{2}mv^2) \quad .$$

Because the ratio of $\Delta_c^o(\frac{1}{2}mv^2)$ to $V\Delta_c(mv)$ is of the order of m/M it is apparent that it is negligible.

To calculate the inelastic momentum operators Shelton employs the frame inveriance of the momentum equation, invariance that is assured by the equation's origin in the second law of Newton. He asserts that

$$\Delta_i^e(mv) = \beta mnV = \Delta_i^h(mv) \quad .$$

Then turning to the energy equation he assumes that ionization is the dominant energy transfer mechanism so that if ν_k is the frequency of the kth inelastic process occurance and E_k is the associated energy, then

$$\sum_k \nu_k E_k \simeq e\phi_i \quad ,$$

where ϕ_i is the ionization potential. Again using frame invariance he finds

$$\Delta_i^e(\tfrac{1}{2}mv^2) = \beta n(\tfrac{1}{2}mV^2 - e\phi_i)$$

and

$$\Delta_i^h(\tfrac{1}{2}mv^2) = \tfrac{1}{2}\beta mnV^2 \quad .$$

The specific nature of β will not enter the solution.

Now Shelton is able to write down analytical forms for the fluid-dynamical equations above. Manipulation of these equations leads to several direct conclusions. First, by combining the heavy particle equations with the ideal gas law and the obvious facts that $M_i = M-m$ for the assumed singly ionized species and that Barions are conserved across the front, he discovers

$$\left[MN_oV_o - mN_iV - \frac{5}{2}\, mN_oV_o\, \frac{kT_i}{mV^2}\right] \frac{dV}{dx} = eN_iE - K_1 mn(v-V)$$

where the zero subscript refers to the region in front of the wave. Inserting order of magnitude values and empirical values for K_1 he finds that $\frac{\Delta V}{V} < 10^{-5}$. This implies that even though electrons and heavy particles transfer the same amount of momentum across the front, the velocity of the heavies appears constant to the electrons. This allows the decoupling of the electron equations from the heavy particle equations.

Second, he discovers a lower limit on the velocity of a wave. This is done by first adding the species equations to get the global equations,

$$MN_oV_o(V-V_o) + mnv(v-V) + N_ok(T_i-T_o) + nkT_e = \frac{\epsilon_o}{2}(E^2-E_o^2)$$

$$MN_oV_o(V^2-V_o^2) + mnv(v^2-V^2) + 5N_oV_ok(T_i-T_o) + 5nvkT_e + nv(2e\phi_i) = 0 .$$

These in turn yield boundary conditions for the wave front (subscripted one) when $n \neq 0$.

$$n_1[v_1(v_1-V_o) + \frac{k(T_e)_1}{m}] = 0$$

$$n_1v_1[v_1^2-V_o^2 + \frac{5k(T_e)_1}{m} + \frac{2e\phi_1}{m}] = 0 \quad .$$

Solving simultaneously gives

$$v_1 = \frac{1}{8}[5V_o-(9V_o^2+16[\frac{2e\phi_1}{m}])^{\frac{1}{2}}] \tag{6}$$

and

$$\frac{k(T_e)_1}{m} = v_1(V_o-v_1) \quad . \tag{7}$$

Knowing that v_1 and V_o are in the same direction and that electron

temperature is obviously positive, then Eq. (6) implies $|V_o| > |v_1|$. Therefore, the limiting condition is

$$\tfrac{1}{2}mV_o^2 > e\phi_i \quad .$$

Third, Shelton solves for the wave speed as a function of applied electric field, E_o, by first writing his equations and boundary conditions in a non-dimensional form. To do this he uses the following substitutions.

$$\nu = \frac{2e\phi_i}{{}_oE_o^2}\, n \qquad \psi = \frac{v}{V} \qquad \theta = \frac{kT_e}{mV^2}$$

$$\varepsilon = \frac{E}{E_o} \qquad \mu = \frac{mV}{eE_o} \qquad \alpha = \frac{2e\phi_i}{mV^2}$$

$$K = \frac{mV}{eE_o}\, K_1 \qquad \xi = \frac{eE_o}{mV^2} = \frac{x}{\lambda} \qquad \lambda < 0$$

Substitution into the electron fluid-dynamical equations and Poisson's leads directly to

$$\frac{d}{d\xi}(\nu\psi) = \mu\nu \tag{8}$$

$$\frac{d}{d\xi}[\nu\psi(\psi-1)+\nu\theta] = -\nu\varepsilon - K\nu(\psi-1) \tag{9}$$

$$\frac{d}{d\xi}[\nu\psi(\psi^2-1)+5\nu\psi\theta+\nu\psi\alpha] = -2\nu\psi\varepsilon - 2K\nu(\psi-1) \tag{10}$$

$$\frac{d\varepsilon}{d\xi} = \frac{\nu}{\alpha}(\psi-1) \quad . \tag{11}$$

The boundary conditions when $\nu_1 \neq 0$ are

$$\psi = \frac{5}{8} - \frac{(9+16\alpha)^{\frac{1}{2}}}{8} \qquad \theta_1 = \psi_1(1-\psi_1) \qquad \varepsilon_1 = 1 \quad .$$

Subtracting two times Eq. (9) from Eq. (10) leads to

$$\nu\psi(\psi-1)^2 + \nu(5\psi-2)\theta + \nu\psi\alpha + \alpha(\varepsilon^2-1) = 0 \quad . \tag{12}$$

Looking far behind the front electron-ion thermal equilibrium assures that $\psi_f \to 1$ while plasma conductivity assures $\varepsilon_f \to 0$ where the subscript f indicates the final value behind the front. Then, Eq. (12) implies

$$\nu_f(\alpha-3\theta_f) = \alpha \ .$$

By equilibrium $\alpha >> \theta_f$ which implies $\nu_f \to 1$ or field energy goes into ionization

$$n_f = \frac{\varepsilon_o E_o}{2e\phi_i} \quad .$$

Then, substituting ε_o times Eq. (11) into Eq. (9), Shelton derives an approximate value for

$$K = \frac{mV}{eE_o} K_1 \simeq \frac{1}{2(1-\psi_1)} + \tfrac{1}{2}\int_{\nu_1}^{1} \frac{\varepsilon^2}{(\psi-1)^2}\, d\psi \simeq \frac{3}{4}\frac{1}{(1-\psi_1)} \quad .$$

Thus, the relation between field and wave speed is

$$V = \frac{eE_o}{mK_1}\frac{3}{4(1-\psi_1)}$$

and substituting ψ_1 we find that V has the form

$$V = AE_o - \frac{B}{E_o} \ .$$

These values for helium are plotted in Fig. 9.

APPENDIX B

TABULATED WAVE SPEED RAW DATA

The table below presents the raw data of distance versus time by listing times in nanoseconds under z the distance down the tube from the electrode. The time interval listed is the elapsed time between the moment when the wave passed a start station at 1.75 m from the electrode and the moment when it passed the stop station at the z value listed. The temporal errors are all uncorrected values indicative of the data spread on the MCA readout, rather than an indication of actual systematic errors. In those cases where recorded errors are less than a nanosecond it merely indicates that the data was extremely spiked. When fractional parts of a nanosecond is recorded for the elapsed time itself, it is only a convenient notation that the distribution was not at all skewed. When the calculations were made to arrive at figures 9 and 10, proper account was taken of significant figures and propagation of error. It was felt, however, that due to the debatable method of data analysis, the actual raw data would be of most value. Applied electrode voltages are always less than 0.5 kV; pressure errors less than two percent on all ranges. Errors in z are less than a millimeter

TIME INTERVAL IN NANOSECONDS FOR WAVE TO GO FROM 1.75 m TO z. Δt versus z.

Press	Volt	z (meters) →								
(Torr)	(kV)	2.25	2.75	3.25	3.75	4.25	4.75	5.25	5.75	6.25
30.1	-42.0	92±1	210±2	344±2	502±2	685±2	903±7	1125±7	1380±7	1577±7
	-36.0	145±2	313±4	496±3	711±7	955±7	1243±7	1550±7	1910±7	
↓ PRO	-30.0	184±2	414±3	680±3	1000±10	1360±10	1766±20			
	-24.0	283±5	653±7	1100±7	1600±7					
	-18.0	530±10	1200±30							
	+42.0	76±3	191±2	332±6	504±6	700±8	905±6	1153±13	1415±13	1695±13
	+36.0	105±3	264±3	462±6	687±9	950±2	1263±2	1563±4		
ANTI	+30.0	156±3	384±8	657±10	970±20	1320±20	1750±20			
	+24.0	253±4	578±8	982±13	1445±26					
	+18.0	600±35	1393±55							
9.8	-42.6	12±1.3	39±0.3	72±3	116±3	164±1	219±1	282±3	353±2	430±2
	-37.2	20±0.6	56±0.6	106±3	164±3	230±2	310±2	395±3	495±3	600±2
↓ PRO	-30.0	35±1	97±1	164±3	253±5	358±5	477±5	610±5	754±5	935±14
	-24.0	66±1	165±4	285±4	433±9	602±9	804±9	1060±20	1310±20	1580±20
	-18.0	130±3		297±5		588±55	590±65	1035±20	1465±35	
	+42.0	18±0.4	46±0.4	78±0.7	117±0.4	160±0.4	211±0.6	264±1	331±1	400±2
	+36.0	24±0.2	58±1	105±1	152±1	210±1	279±1	352±2	444±2	548±2
ANTI	+30.0	34±0.3	82±0.6	139±0.6	208±1	286±2	395±1	510±6	650±6	805±6
	+22.8	60±1	134±1	227±1	350±3	495±6	682±5	904±20	1180±10	
	+18.0	104±3	254±4	430±14	650±14	922±20	1262±35	1625±55		

TIME INTERVAL IN NANOSECONDS FOR WAVE TO GO FROM 1.75 m TO z. Δt versus z

Press (Torr)		Volt (kV)	z (meters) → 2.25	2.75	3.25	3.75	4.25	4.75	5.25	5.75	6.25
2.95	P	-30.0		21±3	23±5	73±6		128±10	156±12		244±12
	R	-18.0	21±3	61±4	116±4	168±7	247±7	315±10		527±15	628±18
↓	O	-13.2	110±8	230±12	345±12	567±25	740±9				
		+42.0		21±1	38.5±1	63±1	87±1	116.5±1	148.5±1	185±3	223±3
	A	+36.0	6±1	27±1	49.5±1	80±4	109±2	151±2	191.5±8	245±4	307±12
	N	+30.0	20±1	41±3	80±4	123±6	176±12	227±9	293±12	370±20	468±30
	T	+25.2	19±2	64±2	100±4	151±4	216±8	290±12	385±18	495±12	640±36
	I										
1.63		-42.0	6±1	19±1	30.5±1	45±2	59±2	75±2	90±2	107±2	175±2
		-36.0	6.5±1	20.5±1	33.5±1	51±1	66.5±2	85±2	101.5±2	121±2	134±2
↓	P	-30.0	8.5±1	25±1	41±1	61±2	82±2	103±3	126±3	150±5	177±5
	R										
	O	-24.0	16±1	38±1	62±2	87.5±2	116±2	144±5	178±5	210±5	248±5
		-18.0	42±2	91±4	145±5	210±5	281±5	364±7	458±7	568±10	695±10
		-12.0	64±20		388±40		847±40	885±130	1090±130	1380±130	1913±250
		+34.2	49±1	112±1	173±2	235±2	301±2	354±3	420±3	485±5	553±5
	A	+30.0	51±1	118±1	182±1	147±1	318±1	375±3	440±3	515±3	587±3
	N	+24.0	57±2	127±2	197±1	268±1	345±3	410±3	490±3	570±3	650±3
	T										
	I	+18.0	71±1	167±3	256±3	352±3	430±6	520±6	630±6	730±6	847±6
		+12.0	113±2	244±4	377±10	528±10	685±15	867±15	1070±3	1263±4	1495±5

TIME INTERVAL IN NANOSECONDS FOR WAVE TO GO FROM 1.75 m TO z. Δt versus z.

Press (Torr)		Volt (kV)	z (meters) → 2.25	2.75	3.25	3.75	4.25	4.75	5.25	5.75	6.25
0.98 ↓	P	-30.0	4±2	24±2	38±4	53±4	69±4	83±4	100±4	115±5	
	R	-18.6	26±4	48±4	68±5	97±6	124±6	150±6	169±6	199±8	288±10
	O	-12.6	31±5	112±5			297±12				
	A										
	N	+34.8	108±10	244±10	362±12	510±12	622±25	643±30	885±30	1005±40	
	T	+20.0	135±10	295±12	428±15	595±15	763±30	943±35	1093±50	1424±70	
	I										
0.30 ↓	P	-39.6	12.5±2	65±4	97±4	126±10	149±8	191±10	215±15	280±15	308±15
	R	-36.0	28±2	70±5	102±5	143±10	168±10	210±10	253±15	291±15	333±15
	O	-20.0	45±3	92±8	138±10	182±12	240±12	287±12	337±20		

APPENDIX C

Raw Temperature Data

```
 10.0      0.03926
HELIUM    5048        89.0    30    360B                                                    360B0
 4.5  7.0  9.0  9.5  9.5  9.0  9.0  9.0  9.0  9.0  9.0  9.0  9.0  9.0  8.5 360B1
 8.0  7.5  7.5  7.0  7.0  6.5  6.5  6.5  6.5  6.0  6.0  6.0  6.0  5.5  5.0 360B2
HELIUM    4713        62.0    30    360B                                                    360B3
 5.5  8.0 11.0 12.5 15.0 17.0 19.0 21.0 22.0 22.0 21.5 19.5 19.0 18.0 17.5 360B4
16.5 16.0 15.5 15.0 14.5 13.0 13.0 12.5 12.0 12.0 11.5 11.0 10.5 10.0 10.0 360B5
 10.0      0.03926
HELIUM    5048        89.0    30    300B                                                    300B0
 5.5  7.0  7.5  8.0  8.0  8.0  8.0  8.0  8.0  8.0  8.0  8.0  8.0  7.5  7.5 300B1
 7.0  7.0  6.5  6.5  6.0  6.0  5.5  5.5  5.0  5.0  4.5  4.5  4.0  4.0  3.5 300B2
HELIUM    4713        62.0    30    300B                                                    300B3
 5.0  8.5 10.5 12.0 13.5 14.5 15.0 15.5 16.0 16.0 16.0 16.0 15.5 15.5 15.0 300B4
15.0 14.5 14.5 14.0 13.5 12.5 12.0 11.0 10.5 10.0 10.0 10.0 10.0 10.0  9.5 300B5
 10.0      0.03926
HELIUM    5048        89.0    30    420C                                                    420C0
 3.0  7.0  8.5  9.0  9.5 10.0 10.0 10.0 10.0 10.5 10.0 10.0  9.5  9.5  9.0 420C1
 8.5  8.0  7.5  7.0  6.5  6.5  6.0  5.5  5.0  5.0  4.0  3.0  2.5  2.0  1.5 420C2
HELIUM    4713        62.0    30    420C                                                    420C3
 5.5 10.0 11.5 13.5 17.5 19.0 21.0 22.0 23.5 24.0 24.5 25.0 24.5 24.0 23.5 420C4
23.5 23.5 23.0 21.5 20.5 19.5 19.0 18.0 16.5 14.5 13.0 12.0 11.5 10.5  9.5 420C5
 10.0      0.03926
HELIUM    5048        89.0    30    360C                                                    360C0
 3.5  6.5  8.5  9.0  9.5  9.0  9.0  9.0  9.0  9.0  9.0  8.5  8.0  7.0  7.0 360C1
 7.0  7.0  7.0  6.0  6.0  6.0  6.0  6.0  5.5  5.0  4.5  4.0  4.0  4.0  3.5 360C2
HELIUM    4713        62.0    30    360C                                                    360C3
```

```
 2.5  5.5  8.0 10.5 13.0 15.0 17.5 18.5 19.0 19.0 19.0 18.5 18.5 18.0 17.5 360C4
17.0 16.5 16.0 15.0 14.5 14.0 13.5 13.0 12.5 11.5 11.0 11.0 10.0  8.0  7.0 360C5
 10.0      0.03926
HELIUM   5048        89.0    30    420D                                      420D0
 8.0 15.0 17.0 16.5 15.5 12.5 12.5 11.5 10.5  9.0  8.5  7.0  6.5  6.0  5.0 420D1
 4.5  4.5  4.0  3.5  3.0  3.0  3.0  2.5  2.5  2.5  2.0  1.5  1.5  1.0  1.0 420D2
HELIUM   4713        62.0    30    420D                                      420D3
 9.0 19.5 26.5 29.0 30.5 30.0 28.5 26.5 25.0 23.0 21.5 20.0 19.0 17.0 15.0 420D4
13.5 13.0 12.5 11.0 10.0  9.5  9.0  8.5  8.0  7.0  6.5  5.5  5.0  4.5  4.0 420D5
 10.0      0.03926
HELIUM   5048        89.0    30    360D                                      360D0
 2.5  5.5 10.0 12.5 12.5 12.5 12.0 11.5 11.0  9.0  8.0  7.5  6.0  5.5  5.0 360D1
 5.0  4.0  3.5  3.0  2.5  2.0  2.0  2.0  2.0  1.5  1.0  1.0  1.0  0.5  0.5 360D2
HELIUM   4713        62.0    30    360D                                      360D3
 8.5 15.0 19.0 20.5 21.5 21.5 21.0 20.0 18.5 17.5 16.0 14.5 13.5 13.0 12.0 360D4
11.5 10.0  9.5  8.5  8.0  7.5  6.5  6.0  5.5  5.0  4.5  4.0  3.5  3.0  3.0 360D5
 10.0      0.03926
HELIUM   5048        89.0    30    300D                                      300D0
 1.5  4.5  8.0 10.5 10.0  9.5  9.0  9.0  8.5  8.5  8.0  7.5  7.0  6.0  5.0 300D1
 5.0  4.5  4.0  3.5  3.5  3.5  3.0  3.0  2.5  2.5  2.0  2.0  2.0  2.0  2.0 300D2
HELIUM   4713        62.0    30    300D                                      300D3
 3.0  7.5 11.0 12.5 13.5 14.0 14.5 14.5 14.0 14.0 13.0 12.0 11.5 10.5 10.0 300D4
 9.0  8.5  7.5  6.5  6.5  6.5  6.5  6.0  6.0  5.5  5.0  4.0  4.0  4.0  4.0 300D5
 10.0      0.03926
HELIUM   5048        89.0    30    420E                                      420E0
 5.0 11.0 14.0 16.5 17.5 17.0 15.5 15.0 13.5 12.0 11.5 10.5  9.5  8.5  8.0 420E1
 8.0  8.0  7.0  6.0  5.0  5.0  4.0  4.0  3.0  3.0  3.0  3.0  3.0  3.0  3.0 420E2
HELIUM   4713        62.0    30    420E                                      420E3
 6.5 14.5 22.5 26.0 29.5 30.5 30.5 29.5 28.5 27.5 26.0 24.0 22.0 20.5 19.5 420E4
19.0 17.5 16.0 15.0 14.0 13.5 12.0 11.0 10.0  9.0  8.5  8.0  8.0  7.5  7.0 420E5
```

```
 10.0      0.03926
HELIUM    5048        89.0    30    348E                                                    348E0
 4.0  7.0 20.0 12.0 13.0 12.5 12.0 11.0 10.5  9.5  8.5  8.0  7.0  6.5  6.0 348E1
 5.5  5.0  4.5  4.0  3.5  3.0  2.0  2.0  2.0  1.5  1.5  1.0  1.0  1.0  1.0 348E2
HELIUM    4713        62.0    30    348E                                                    348E3
 5.0 11.0 15.0 19.0 21.0 21.5 22.0 21.5 20.5 19.0 18.0 17.0 16.0 14.5 14.0 348E4
12.5 11.5 11.0 11.0 10.0  9.0  8.5  8.0  7.0  6.5  6.0  5.0  4.5  4.5  4.0 348E5
 10.0      0.03926
HELIUM    5048        89.0    30    300E                                                    300E0
 5.0  6.5  8.0  8.5  9.0  9.5  9.0  8.5  8.0  7.5  7.0  6.5  6.0  5.5  5.0 300E1
 4.5  4.0  4.0  3.0  3.0  3.0  2.5  2.0  2.0  2.0  2.0  2.0  2.0  1.5  1.5 300E2
HELIUM    4713        62.0    30    300E                                                    300E3
 5.0  8.0 10.5 14.0 15.0 16.0 16.0 16.0 15.5 15.0 14.5 14.0 13.5 13.0 13.0 300E4
12.0 11.5 11.0 10.0  9.0  8.0  7.0  7.0  6.0  5.5  5.5  5.0  5.0  5.0  4.5 300E5
 10.0      0.03926
HELIUM    5048        89.0    30    420E                                                    420E0
 6.0 12.5 19.0 21.5 23.5 24.0 24.0 23.0 22.5 21.0 19.5 16.5 15.5 14.5 13.5 420E1
12.0 11.0  8.5  7.5  6.0  4.5  3.5  2.5  2.5  2.5  2.5  2.5  2.5  2.5  2.5 420E2
HELIUM    4713        62.0    30    420E                                                    420E3
 9.5 19.5 28.0 32.5 36.0 39.0 40.5 40.5 40.5 39.5 39.0 38.5 37.5 35.0 34.0 420E4
31.0 27.5 24.0 22.5 21.0 19.0 17.0 15.0 14.0 13.5 12.0 11.0 10.0  9.5  9.0 420E5
 10.0      0.03926
HELIUM    5048        89.0    30    360E                                                    360E0
 2.5  7.5 13.0 17.0 18.5 19.5 19.5 19.0 19.0 18.5 17.5 16.5 15.5 14.5 13.5 360E1

13.0 12.0 11.5 10.0  9.0  8.5  7.5  7.0  6.0  5.0  5.0  4.5  4.5  4.5  3.5 360E2
HELIUM    4713        62.0    30    360E                                                    360E3
 4.0 11.5 16.5 21.5 24.0 27.0 28.0 28.0 27.0 26.0 24.5 24.0 23.0 21.5 20.5 360E4
19.5 18.5 17.5 16.5 14.5 13.5 12.0 11.5 10.5  9.5  8.5  7.5  7.0  6.5  6.0 360E5
 10.0      0.03926
HELIUM    5048        89.0    30    300E                                                    300E0
 3.0  6.0  8.5 10.0 11.0 11.5 11.5 11.5 11.0 10.0  9.5  9.5  9.5  9.5  9.5 300E1
 9.0  9.0  9.0  8.5  8.0  8.0  7.5  7.5  7.0  7.0  7.0  7.0  7.0  6.5  6.5 300E2
HELIUM    4713        62.0    30    300E                                                    300E3
 5.0  8.5 11.0 12.0 14.0 16.5 17.0 17.5 17.0 16.5 16.0 15.5 15.5 15.0 14.0 300E4
14.0 13.0 12.5 12.0 12.0 11.0 10.5 10.5 10.0 10.0  9.5  9.0  8.0  8.0  7.0 300E5
```